Intracranial tumors elicit systemic sympathetic hyperactivity that limits immunotherapeutic responses

Selena J. Lorrey[+1,2], Lucas P. Wachsmuth[+2,3,4], John B. Finlay[4,5], Jessica Waibl Polania[2,3], Alexandra Hoyt-Miggelbrink[2,3], Mackenzie Price[6], Corey Neff[6], Xiuyu Cui[2,6], Amelia Hawley[7], Emily Lerner[2,8,9], Daniel Wilkinson[2,6], Ethan Srinivasan[2,9], Quinn T. Ostrom[6], Peter E. Fecci*[1,2,3,6,8,9]

[+]contributed equally
*corresponding author peter.fecci@duke.edu

1. Department of Integrative Immunobiology, Duke University, Durham, NC, USA
2. Brain Tumor Immunotherapy Program, Duke University, Durham, NC, USA
3. Department of Pathology, Duke University, Durham, NC, USA
4. Medical Science Training Program, Duke University, Durham, NC, USA
5. Department of Cell and Molecular Biology, Duke University, Durham, NC, USA
6. Department of Neurosurgery, Duke University, Durham, NC, USA
7. Duke University, Durham NC, USA
8. Department of Biomedical Engineering, Duke University, Durham, NC, USA
9. School of Medicine, Duke University, Durham, NC, USA

Author Contributions:
SJL and LPW conceived and designed experiments. SJL, LPW, JWP, AHM, XC, AH, acquired data. SJL, LPW, JBF, MP, CN, QTO analyzed data. SJL, LPW and PEF interpreted data. SJL, LPW and PEF wrote the manuscript. EL, DW, ES provided feedback.

Acknowledgements:
Dr. Fecci is the recipient of a CRI Arash Ferdowsi Lloyd J. Old STAR grant, which helped to fund this work. We thank Kyle Walsh and Gary Archer from the Duke University Brain Tumor Center for providing human serum samples. We further thank Amanda van Swearingen from the Duke University Center for Brain and Spine Metastases for IRB protocol assistance. We thank the Duke University School of Medicine for the use of the Microbiome Core Facility that provided the Nanostring Gene Expression service. This study used the linked SEER-Medicare database, and we thank Zhen Liu for her assistance with data analysis. The interpretation and reporting of these data are the sole responsibility of the authors. The authors acknowledge the efforts of the National Cancer Institute; Information Management Services (IMS), Inc.; and the Surveillance, Epidemiology, and End Results (SEER) Program tumor registries in the creation of the SEER-Medicare database. The collection of cancer incidence data used in this study was supported by the California Department of Public Health pursuant to California Health and Safety Code Section 103885; Centers for Disease Control and Prevention's (CDC) National Program of Cancer Registries, under cooperative agreement 1NU58DP007156; the National Cancer Institute's Surveillance, Epidemiology and End Results Program under contract HHSN261201800032I awarded to the University of California, San Francisco, contract HHSN261201800015I awarded to the University of Southern California, and contract HHSN261201800009I awarded to the Public Health Institute. The ideas and opinions expressed herein are those of the author(s) and do not necessarily reflect the opinions of the State of California, Department of Public Health, the National Cancer Institute, and the Centers for Disease Control and Prevention or their Contractors and Subcontractors. Schematics in Fig.1, 3 and 4 were created with BioRender.com.

ABSTRACT

Intracranial tumors present unique challenges for immunotherapy, which can include both local and systemic immune suppression whose mechanistic underpinnings are incompletely understood. Here, we reveal that tumors harbored intracranially elicit systemic increases in catecholamines and chronic sympathetic hyperactivity that drives T cell dysfunction and limits immunotherapeutic success. Conversely, treatment with β-adrenergic receptor blockade increases NF-κB activity in immune cells**,** restores T cell polyfunctionality, modifies the tumor microenvironment, and licenses immune-based therapies in murine models of GBM to extend survival. Extended survival was also observed in GBM patients receiving β-blockers for any indication, as well as in patients with melanoma and lung cancer brain metastases who received concomitant immune checkpoint inhibition and β-adrenergic blockade compared to immune checkpoint inhibition alone. These data suggest roles for increased adrenergic activity in facilitating systemic immune dysfunction in the setting of intracranial tumors, specifically, and advance a role for β-adrenergic blockade in licensing immunotherapeutic responses within the intracranial compartment.

INTRODUCTION

Glioblastoma (GBM) is the most common primary brain malignancy and remains nearly uniformly lethal. While modern immunotherapeutic approaches enjoy success against a variety of solid tumors, GBM persists as a notable exception[1-3]. Contributing to treatment failures is a remarkable degree of both local and systemic immune dysfunction, despite the fact that GBM remains confined to the intracranial compartment. Particularly prominent are multiple modes of long-characterized T cell dysfunction, all capable of hindering the antitumor response[4-27]. In addition, GBM elicits various systemic derangements afflicting the peripheral immune compartments, including lymphopenia, primary and secondary lymphoid organ atrophy, and sequestration of T cells in the bone marrow[4,20-22,26-28]. We now know these derangements are not specific to GBM but instead accompany various tumors when situated in the intracranial compartment. Lung, melanoma, and breast cancers all elicit comparable immune dysfunction, for instance, but only when these tumors are harbored within the brain[20].

Herein we report that intracranial tumors of varying histology (but not their peripheral counterparts), evoke dramatic increases to levels of circulating catecholamines in both patients and mice, which in turn drive loss of critical T cell functions. Further**,** catecholamine infusions into naïve mice are sufficient to recapitulate the same T cell deficiencies observed in the setting of IC tumors. While catecholamines signal through both α- and β-adrenergic receptors, lymphocytes are shown to express predominantly β2-adrenergic receptors. In a variety of contexts, β2-adrenergic signaling has been shown to suppress immune cell function via inhibition of nuclear factor kappa B (NF-κB) activity[29-34]. Consequently, we find that treatment with β-adrenergic receptor blockade increases NF-κB activity in immune cells**,** restores T cell polyfunctionality, modifies the tumor microenvironment (TME), and licenses immune-based therapies in murine models of GBM to newly elicit long-term survival. Furthermore, large scale analysis of Medicare data reveals that extended survival is found in GBM patients receiving β-blockers for any indication, as well as in patients with melanoma and lung cancer brain metastases who receive concomitant immune checkpoint inhibition and β-adrenergic blockade, as compared to checkpoint inhibition alone. These data suggest critical roles for increased adrenergic activity in facilitating systemic immune dysfunction in the setting of intracranial tumors, specifically, and advance a role for β-adrenergic blockade in licensing immunotherapeutic responses within the intracranial compartment.

RESULTS

Tumors elicit elevations in circulating catecholamine levels when situated within the intracranial compartment

In an effort to investigate a role for the sympathetic nervous system (SNS) in mediating the systemic immune deficits observed in patients with GBM, we assessed serum catecholamine levels in patients with either newly diagnosed or recurrent GBM, as well as in sex-matched healthy controls **(Fig. 1A)**. Newly diagnosed **(Fig. 1B)** and recurrent **(Fig. 1C)** GBM patients each exhibited substantial elevations in circulating levels of both epinephrine and norepinephrine. Extending these studies to a murine model of high-grade glioma, we collected sera and spleens from immunocompetent C57BL/6 mice bearing syngeneic intracranial CT2A glioma (CT2A) and compared catecholamine levels to those in mice that had instead received sham tumor implantations **(Fig. 1D-F).** Catecholamine levels were elevated in both the serum **(Fig. 1E)** and spleens **(Fig. 1F)** of mice bearing intracranial CT2A, recapitulating findings in patients with GBM.

Intrigued, we examined whether rising systemic catecholamine levels were: 1) specific to GBM alone; 2) elicited by tumors of the intracranial compartment; or 3) a feature of cancer more generally. We began by implanting CT2A into either the brain (intracranial, IC) or the flank (subcutaneous, SubQ) of C57B/6 mice. Systemic elevations in epinephrine and norepinephrine levels followed only when CT2A was introduced intracranially, suggesting a phenomenon specific to the intracranial compartment **(Fig. 1G)**. To investigate whether catecholamine rises were specific to GBM, we instead implanted B16 melanomas (B16) **(Fig. 1H)** or Lewis lung carcinomas (LLC) **(Fig. 1I),** again into either the brains or flanks of C57BL/6 mice. While increased epinephrine and norepinephrine levels accompanied all tumor histologies, such increases occurred exclusively when the respective tumors were situated intracranially **(Figs. 1G-I)**.

β2-adrenergic receptors are the predominant subtype found within the intracranial TME, as well as on circulating immune cells

Epinephrine and norepinephrine signal through both α- and β-adrenergic receptors. To determine which receptors might be mediating any immunologic impact of increased catecholamine levels, we interrogated publicly available single cell RNA sequencing (scRNAseq) datasets and analyzed the expression of α-and β-adrenergic receptor subtypes on tumor cells, as well as on circulating and tumor-infiltrating immune populations. Our dataset was generated by integrating scRNAseq data from human samples that included healthy brain (n=5), newly-diagnosed GBM (n=24), recurrent GBM (n=17), low grade glioma (n=2), melanoma brain metastasis (n=8), breast cancer brain metastasis (n=3), lung cancer brain metastasis (n=3), healthy donor peripheral blood mononuclear cells (PBMC) (n=2), and PBMC from patients with GBM (n=5) **(Fig. 2A)**. Healthy brain tissue was also assessed **(Supplementary Fig. 2)**. After performing quality control, normalization, and integration, this dataset ultimately consisted of 552,442 cells. Clustering was performed and cells were visualized by Uniform Manifold Approximation and Projection (UMAP), yielding cell type-specific clusters that included tumor-, immune-, and brain-resident-cells **(Fig. 2B)**. Examination of clustering by patient **(Supplementary Fig. 1A)** and by tissue of origin **(Supplementary Fig. 1B)** demonstrated successful integration, with no evidence of batch effects. Clusters were identified and annotated according to their expression of signature population-defining genes.

Focusing first on PBMCs, healthy donor PBMC profiles were found to consist of mainly myeloid and lymphoid clusters **(Fig. 2C),** which predominantly expressed the β2-adrenergic receptor (*ADRB2*). Low expression levels of β1-adrenergic receptors (*ADRB1*) were also seen, while

expression of α- and β3-adrenergic receptors was negligible **(Fig. 2D)**. Lymphoid cells demonstrated significantly higher expression of *ADRB2* than myeloid cells **(Fig. 2E)**. PBMCs from patients with GBM yielded comparable findings **(Fig. 2F-H)**.

Repeating these analyses on tumor samples, clustering of newly diagnosed and recurrent GBM samples each revealed population subsets corresponding to tumor cells, microglia, myeloid cells, and lymphoid cells **(Fig. 2I)**. Feature plots demonstrated that the β2-adrenergic receptor was again the predominant adrenergic receptor present across all clusters, with minimal to negligible expression of the other receptor subtypes observed **(Fig. 2J)**. Likewise, lymphoid, myeloid, and microglial cells were the highest expressers of the β2-adrenergic receptor, while receptor expression was essentially absent on tumor cells **(Fig. 2K)**. Similar findings were uncovered in brain metastases **(Fig. 2L-N)**. Examination of feature plots of adrenergic receptor expression in healthy brain tissue demonstrated minimal expression of all receptors except for α1 (*ADRA1A* and *ADRA1B*), which was found to be concentrated in neurons and astrocytes (**Supplementary Fig. 2A**). While expression levels of β-adrenergic receptors in healthy brain were found to be quite low, comparison of the relative expression of β1- and β2-adrenergic receptors specifically indicated that astrocytes and microglia, respectively, were the cell populations with the highest expression of these two receptors (**Supplementary Fig. 2B)**.

Systemic T cell function is impaired by catecholamine surges and restored by β-adrenergic blockade in the setting of intracranial tumors

We next sought to evaluate the contribution of elevated catecholamine levels to T cell dysfunction, which has been extensively characterized in the context of GBM. Historically, studies have reported diminished T cell reactivity, often demonstrating limited proliferative and cytokine responses [4-6,8,9,14,16-19,24,26,27,35-41]. More current techniques assess multiple cytokines simultaneously to address T cell "polyfunctionality",[42-53] which has been linked to outcomes in various tumor types[54-56]. We thus used a high-throughput, ELISA-based single-cell cytokine secretion assay to assess T cell polyfunctionality and compared systemic T cell function in the setting of both intracranial and peripheral tumors. Splenic T cells from naïve mice or from mice with either intracranial or subcutaneous GBM were isolated and stimulated *ex vivo* with anti-CD3/anti-CD28 antibodies for 48 hours. T cell production of Granzyme B, IFNγ, MIP-1α/CCL3, IP-10/CXCL10, RANTES/CCL5, IL-27, sCD137/4-1BB, IL-21, IL-17 and IL-6 was then assessed **(schematic in Fig. 3A).** As anticipated, $CD8^+$ T cells from mice with intracranial GBM exhibited diminished polyfunctionality with regard to both frequency **(Fig. 3B)** and strength of response **(Fig. 3C),** compared to either naïve or subcutaneous GBM-bearing mice. We further examined the strength of Granzyme B production, as this cytokine is a hallmark of $CD8^+$ T cell cytotoxicity and the capacity to produce Granzyme B is critical to anti-tumor immunity[57,58]. We observed a decreased capacity to produce Granzyme B in CD8+ T cells from mice with intracranial GBM compared to naïve mice or mice with subcutaneous GBM **(Fig. 3D)**.

As intracranial tumors are marked by both pronounced T cell dysfunction and elevated catecholamine levels, we assessed whether increased catecholamine levels are sufficient to elicit T cell functional deficits. Using the same polyfunctionality assay, we evaluated splenic $CD8^+$ T cells from naïve mice, mice with intracranial tumors, or naïve mice with an implanted peripheral catecholamine pump. Systemic high dose catecholamine infusion proved sufficient to impair T cell function in much the same manner as intracranial tumors **(Fig. 3E-G).** As T cells were seen to predominantly express β2-adrenergic receptors **(Figs. 2C-H),** we evaluated whether β2-adrenergic agonism, more specifically, was likewise sufficient to drive T cell dysfunction. Indeed, T cells from mice treated with the β2-adrenergic agonist salbutamol exhibited severely reduced functional capacity **(Fig. 3 H-J).** Further, treatment of orthotopic CT2A-bearing mice with the

nonselective β-adrenergic blocker propranolol significantly restored polyfunctional T cell responses that were suppressed in the setting of GBM **(Fig. 3 K-M).** Treatment with propranolol did not, however, prevent systemic immune derangements such as lymphoid organ atrophy T cell sequestration) and lymphopenia **(Supplementary Fig. 3)**. In addition, treatment with propranolol decreased immunosuppressive cytokine production in CT2A-bearing mice, including $CD4^+$ T cell production of IL-10 and TGFβ (regulatory T cell cytokines) (**Fig. 3N).** Populations of T cells producing multiple immunosuppressive cytokines were also diminished **(Fig. 3O dotted circle).** Notably, there was no significant differences in the composition of various immune compartments **(Supplementary Fig. 4).**

β-adrenergic blockade proffers a pro-inflammatory intracranial TME

Many of the proinflammatory cytokines impacted by adrenergic activity above (Granzyme B, IFNγ, MIP-1α/CCL3, sCD137/4-1BB, and RANTES/CCL5) are regulated by NF-κB. Interestingly, β2-adrenergic receptor signaling is known to suppress NF-κB activity and thus inhibit inflammatory responses in the setting of other intracranial pathologies, such as stroke[59]. We therefore sought to understand the impact of β-adrenergic blockade within the intracranial TME, as well as to investigate any influence on NF-κB-mediated activity. Mice with intracranial CT2A were administered either 0.5g/L propranolol or vehicle control in drinking water *ad libitum* beginning on the day of tumor implantation (Day 0). Upon clinical decline, intracranial tumors were harvested for analysis. Tumor-infiltrating leukocytes (TILs) were sorted and enriched for either T cells or for APC prior to bulk RNA-sequencing **(schematic in Fig. 4A).**

As T cell exhaustion is a well-established form of T cell dysfunction in the TME[60,61], we first assessed the impact of propranolol on T cell differentiation states and observed that transcript levels of the classical exhaustion markers *Lag3*, *Havcr2* (Tim3) and *Pdcd1* (PD-1) trended lower in mice treated with propranolol **(Supplementary Fig. 5)**. T cells from mice treated with propranolol, however, did harbor significantly decreased *Nfkbia* (IkBα) transcript levels **(Fig. 4B).** IkBα is the "inhibitor of NF-κB" that is degraded upon activation of the canonical NF-κB signaling pathway[62]. In T cells from the TME, propranolol likewise resulted in a striking increase in IL-2 transcript levels and trending increases in transcript levels of *IL-1β* and *CD40L*, each of which are canonical downstream NF-κB targets **(Fig. 4C).** As NF-κB activation is required for T cell priming[63], we also assessed the transcript levels of downstream NF-κB target genes in the APC-enriched samples and observed increases in IL-12, CD40, and CD80 transcripts **(Fig. 4D)**, all of which are expressed by dendritic cells (DCs). We further found that APCs exhibited increased transcript levels of the NF-κB subunits *c-Rel* and *Relb*, highly suggestive of increased NF-κB activity (**Fig. 4E).**

In addition to transcript levels, we assessed changes within the TME at the protein level via flow cytometry **(schematic in 4F; Gating strategy in supplementary Fig. 6).** Treatment with propranolol elicited no marked differences in the relative immune cell composition of the TME **(Fig. 4G)** but did increase the number of tumor-infiltrating immune cells overall **(Fig. 4H).** These increases were driven by enhanced numbers of conventional type 1 dendritic cells (cDC1s; subset of DCs critical for T cell priming and $CD8^+$-mediated cytotoxicity[64,65]) **(Fig. 4I**) and $CD8^+$ T cells **(Fig. 4J)**, but not $CD4^+$ T cells **(Fig. 4K)**. Given the requirement of NF-κB activation for T cell priming and the upregulation of both CD40 and CD40L transcript levels, we examined the capacity of T cells to interact with APCs via the CD40/CD40L axis.[66,67] We found that propranolol increased the number of $CD40L^+$ T cells in the TME **(Fig. 4L)** as well as the mean expression levels of CD40L per T cell **(Fig. 4M)**. Additionally, we examined the degree of CD40 expression on cDC1s

as a surrogate for T cell priming capacity. Treatment with propranolol not only increased the number of cDC1s expressing CD40 **(Fig. 4N)**, but also the mean CD40 levels per cDC1 **(Fig. 4O)**.

Treatment with β-adrenergic blockade enhances the response to immunotherapy in mice and patients with intracranial tumors

Seeing benefits to both systemic and local immune functions, we next examined whether β-adrenergic blockade could improve immunotherapeutic responses within the intracranial compartment and meaningfully prolong survival. Mice with intracranial CT2A were again administered propranolol vs. vehicle control in drinking water starting day 0 and then treated with a T cell-activating 4-1BB agonist antibody vs. control on days 9, 12, 15 and 18 post-tumor implantation. The combination of propranolol and immunotherapy licensed long-term survival, where none was previously seen with either treatment alone **(Fig. 5A)**. We found no significant difference in survival whether propranolol administration began on day 0 or day 7 post-tumor implantation (p=0.592) **(Fig. 5B)**, suggesting that propranolol maintains the capacity to license immunotherapeutic responses even after tumor is well-established.

To assess whether such findings might be relevant in patients with intracranial cancers, we utilized the Surveillance, Epidemiology and End Results (SEER)-Medicare database to retrospectively assess the impact of β-blockade therapy (prescribed for any indication) on outcome in patients with GBM (see inclusion and exclusion criteria in **Table 1**). As no immunotherapies are currently FDA-approved in GBM, they are not insurance-reimbursed, and thus no data on the combination of β-blockade and immunotherapy are currently available through the SEER-Medicare database. We were, however, able to assess the impact of β-blockade monotherapy in patients with GBM. For the purposes of this retrospective study, a total of 8,723 patients met criteria, after excluding patients younger than 65 years at the time of diagnosis (as recorded in SEER data) and those enrolled due to end-stage renal disease or disability. Patients enrolled in a health maintenance organization (HMO) 6 months prior to and 12 months after primary diagnosis were also excluded (see demographics in **Table 2)**. Of these 8,743 patients, 655 had been prescribed β-adrenergic blockade (for any indication) at the time of their cancer diagnosis (**Fig. 5C)**. Median overall survival (OS) of GBM patients receiving β-adrenergic blockade (14 months) was significantly extended by more than 25% compared to those who did not (11 months) (p=<0.0001) **(Fig. 5D)**. Interestingly, a similar survival extension was observed across experiments prospectively employing β-adrenergic blockade as a monotherapy in mice with intracranial CT2A (n= 43-47 per group, p=0.032) **(Fig. 5E).**

In contrast to GBM, immunotherapies (checkpoint blockade, in particular) are FDA-approved in patients with brain metastases from melanoma and from certain lung cancers, permitting us to identify patients with these conditions who may have been treated with immunotherapy and β-adrenergic blockade simultaneously. We therefore returned to the SEER-Medicare database to retrospectively determine survival outcomes in patients with melanoma or lung cancer brain metastases who had received immunotherapy alone for their cancer versus those who had received immunotherapy concomitantly with β-adrenergic blockade (the latter again for any indication).

We assessed patients with melanoma brain metastases meeting the inclusion criteria above for GBM but also receiving checkpoint blockade (n=510). Of these, 104 patients were also on a β-blocker **(Fig. 5F)**. Patients receiving a combination of β-blockade and checkpoint blockade therapies exhibited a 40% increase in median OS over those receiving checkpoint blockade alone (35 months vs 25 months, p=0.006) **(Fig. 5G).**

In patients with lung cancer brain metastases meeting the same criteria (n=1,074), 267 had received concomitant β-blocker and checkpoint blockade **(Fig. 5H)**. Similar to melanoma patients, lung cancer patients with brain metastases receiving the combination of both therapies exhibited a 31% increase in median OS compared to those receiving checkpoint blockade alone (25 months vs 19 months; p=0.013) **(Fig. 5I)**. Further, cox-proportional hazard ratios were calculated for GBM, melanoma and lung cancer **(Table 3).**

DISCUSSION

Immunotherapy for intracranial tumors, particularly GBM, has proven difficult to successfully implement, especially when compared to outcomes in extracranial disease. Historically, this failure in intracranial disease has been attributed to factors such as central nervous system (CNS) immune privilege[68], the blood-brain barrier (BBB)[69], and immunosuppressive features of the intracranial TME[70,71]. Here, however, we identify a role for sympathetic hyperactivity as a novel driver of local and systemic immune dysfunction in the setting of intracranial tumors. This sympathetic hyperactivity, manifesting as elevated catecholamine levels and increased β-adrenergic signaling, accompanies intracranial tumors in a histology-agnostic fashion.

The immunosuppressive nature of SNS hyperactivity has been well-documented[72]. Further, elevated systemic catecholamine levels have been described in the setting of other intracranial pathologies, such as stroke, where they have been associated with "stroke-induced immunodepression syndrome" (SIDS)[73]. Studies suggest that SIDS may be attributable to inhibition of NF-κB activity, which is in turn mediated by β-adrenergic signaling[74]. However, to our knowledge, this is the first study investigating a role for this immunosuppressive axis in intracranial tumors. We report here that elevated catecholamines, increased β-adrenergic activity, and diminished NF-κB-mediated immune functions are each also observed in the setting of intracranial tumors and are sufficient to induce much of the T cell dysfunction found amidst GBM. As these observations span multiple intracranial, but not extracranial, pathologies, this suggests a shared axis through which the CNS restricts systemic immune responses following inflammatory insults, an axis utilized by intracranial tumors to foster their immune escape. Further investigation into the upstream mechanistic underpinnings of sympathetic hyperactivity in these settings is warranted.

Systemic immune dysfunction imposed specifically by intracranial tumors is reversible and can be restored simply by employing β-adrenergic blockade using propranolol. We report that propranolol reinstates the capacity of systemic T cells to respond in a polyfunctional manner to immune stimuli and increases NF-κB activity in both T cells and APCs within the TME. Critical for anti-tumor immunity, propranolol both increases the numbers of $CD8^+$ T cells and cDC1s at the tumor and enhances their CD40L and CD40 expression, respectively. CD40 expression on cDC1s is increasingly viewed as an important surrogate for dendritic cell activation,[75] which is crucial for both $CD8^+$ T cell priming and subsequent tumor rejection[76,77]. cDC1s are positively correlated with survival and responsiveness to immunotherapy in cancer patients[78-81] and CD40 has been proposed as an adjuvant to immunotherapy[75]. In GBM, specifically, higher expression of CD40/CD40L has correlated with improved patient outcomes[82]. Our data therefore reveal that β-blockade is capable of restoring multiple components critical to an effective anti-tumor immune response in intracranial tumors. Given the severe systemic and local immunosuppression unique to intracranial malignancies, β-blockade may represent a powerful adjunct to immunotherapy for the treatment of intracranial tumors. Indeed, our murine survival studies demonstrate

propranolol's capacity to license immunotherapies that were previously ineffective against glioma and result in long-term survival.

Importantly, our studies highlight the impact of β-adrenergic blockade on local and systemic immune responses, and not directly on tumor cells. Several studies have examined the direct *in vitro* inhibitive effects of propranolol on glioma cell lines[83-86], although our data reveal relatively low expression of β-adrenergic receptors on tumor cells compared to the immune compartment. Likewise, there is only a single study investigating the translational relevance of glioma adrenergic receptor expression. That study retrospectively assessed outcomes in patients (n=243 total) with recurrent GBM and revealed no association between β-blockade and overall survival[87]. In contrast, our analysis of the SEER-Medicare database investigated a total patient cohort nearly 35 times larger and included newly diagnosed GBM patients.

Beyond the limited studies in GBM, there have been several clinical studies investigating the impact of β-adrenergic blockade on survival in melanoma. To date, these have demonstrated conflicting results[88-91]. Furthermore, much of the current work has focused on β-adrenergic blockade as a monotherapy[92-94]. Those studies assessing combinations of β-adrenergic blockade with immunotherapy frequently have excluded patients with stage IV disease, thereby excluding patients with brain metastasis[95-98]. While these studies provide mixed evidence regarding the impact of β-adrenergic blockade monotherapy on survival, there is a mounting body of evidence indicating that β-blockers are an effective adjunct to immunotherapy in the setting of peripheral disease[99]. The key distinction between extracranial and intracranial tumors demonstrated herein, however, is the unique increase in systemic catecholamine levels found accompanying intracranial tumors. Although extracranial tumors may exhibit elevated catecholamine levels within the TME that prove locally immunosuppressive[93,94], they do not elicit the systemic sympathetic hyperactivity and T cell dysfunction seen with their intracranial counterparts. Likewise, the impact of β-blockade for extracranial tumors is likely restricted to the TME, while the benefits of β-blockade in the setting of intracranial malignancies is both more systemic and more pronounced.

While our data examining survival in patients with GBM and intracranial melanoma and lung metastases are retrospective and limited by the bias of indication, the complement proffered by our murine survival and immune data strongly suggest a novel and specific benefit to combining β-adrenergic blockade and immunotherapy in the setting of intracranial tumors. Our studies examining patients with brain metastases are particularly relevant, as lung cancer and melanoma have two of the highest rates of intracranial metastasis[100,101], which are now nearly 10 times more prevalent than GBM. Our data support the initiation of prospective randomized controlled trials to examine the addition of β-adrenergic blockade to immunotherapeutic regimens in patients with intracranial cancers, whether primary or metastatic. Such trials, we anticipate, will be viewed favorably, as β-blockers are FDA-approved, relatively inexpensive, and have exhaustively established safety profiles[102]. Repurposing β-blockers as an immunotherapeutic adjunct may ultimately represent a novel intervention for licensing long-sought after effective immune responses within the intracranial compartment.

METHODS

Mice

The Institutional Animal Care and Use committee (IACUC) at Duke University Medical Center approved all experimental procedures. Female C57BL/6 mice purchased from Charles River Laboratories were purchased at 5-6 weeks of age. Animals were maintained under specific

pathogen-free conditions at the Cancer Center Isolation Facility of Duke University Medical Center. All experimental procedures were approved by the Institutional Animal Care and Use Committee.

Cell lines

Murine CT-2A malignant glioma was kindly provided by Robert L. Martuza (Massachusetts General Hospital, MA, USA). LLC1/2 lung adenocarcinoma were purchased from the American Tissue Culture Collection (ATCC). Murine B16F0 melanoma was obtained from the Duke Cell Culture Facility but is also available from ATCC. All cell lines are syngeneic on the C57BL/6 background. CT-2A and LLC1/2 were grown *in vitro* in Dulbecco's Modified Eagle's Medium (DMEM) with 2mM L-glutamine and 4.5mg ml^{-1} glucose (Gibco) containing 10% fetal bovine serum (FBS) (Sigma). B16F0 cells were grown *in vitro* in DMEM with 4mM L-glutamine, 4.5mg ml^{-1} glucose, 1mM sodium pyruvate, 1500 mg/L sodium bicarbonate containing 10% FBS (Sigma). Cells were collected in the logarithmic growth phase. All cell lines were authenticated and tested negative for mycoplasma and interspecies contamination by IDEXX Laboratories.

Tumor Implantation

For intracranial implantation, tumor cells were resuspended at a given concentration in PBS, then mixed 1:1 with 3% methylcellulose and loaded into a 250μL syringe (Hamilton). Prior to injection, mice were anesthetized with isoflurane and subject to an anteroposterior incision to reveal the skull. The needle was positioned 2mm to the right of the bregma and 4mm below the surface of the skull at the coronal suture using a stereotactic frame. $1e^4$ CT-2A, $1e^3$ B16F0 or $1e^3$ LLC1/2 cells were delivered in a total volume of 5μL per mouse. For subcutaneous implantation, $5e^5$ CT2A, $2.5e^5$ B16F0, or $5e^5$ LLC1/2, were injected in a total of 200μL of PBS into the subcutaneous tissues of the left flank.

Catecholamine ELISAs

Blood and spleen were collected from non-tumor bearing, intracranial-tumor bearing or subcutaneous-tumor bearing mice at humane endpoint. Mice were anesthetized using isoflurane then subject to retro-orbital bleed and subsequent euthanasia and tissue harvest. Blood samples were centrifuged at 2000g for 15min at 4°C to isolate plasma then plasma was isolated in 58.8μL aliquots with 1.2μL 50mM EDTA 200mM sodium metabisulfite per sample to protect against catecholamine degradation. Spleens were collected into 500μL of a PBS/ 50mM EDTA 200mM sodium metabisulfite solution, weighed, homogenized through 70μm filters, washed with an addition 500μL of PBS/EDTA/sodium metabisulfite solution for a total of 1mL then centrifuged at 500g for 5min at 4°C. Supernatants were collected by combining 58.8μL supernatant and 1.2μL 50mM EDTA 200mM sodium metabisulfite into Eppendorf tubes. All samples, including human serum samples were stored at -80°C. Epinephrine and norepinephrine levels in plasma, serum, and spleen supernatant were analyzed using the 2-CAT (A-N) Research ELISA (Rocky Mount Diagnostics).

Murine tissue harvest

Tumor, spleen, thymus, inguinal or deep cervical lymph node, and tibia were collected at defined and/or humane endpoints, in accordance with protocol. For intracranial tumor-bearing animals, humane endpoints include inability to ambulate two steps forward with prompting. For subcutaneous tumor-bearing animals, humane endpoints include tumor size greater than 20 mm in one dimension, $2000mm^3$ in total volume, or tumor ulceration or necrosis. Spleens, lymph nodes and thymi were weighed. Briefly, tissues were processed in RPMI or PBS, minced into

single cell suspensions, cell-strained, counted, stained with antibodies, and analyzed via flow cytometry.

Tumors were mechanically homogenized using a Dounce Tissue Homogenizer and enzymatically digested using 0.05mg ml^{-1} Liberase TL (Roche), 0.2mg ml^{-1} Dnase I (Roche) in HBSS with calcium and magnesium. Tumors in digestion buffer were then incubated at 37C for 15min, PBS was used to quench the enzymatic reaction, and tumors were filtered (70um). After centrifugation, cells were resuspended in 1x RBC Lysis Buffer (eBioscience) for 3min and quenched with PBS. Samples were subsequently centrifuged then resuspended in 30% Percoll (Sigma Aldrich) and centrifuged at 500g for 20min at 18°C with a low brake. The myelin-containing supernatant was then aspirated and the cell pellet resuspended in PBS for staining.

Blood was collected into EDTA tubes and mixed thoroughly to prevent coagulation. After collection, 75μL of each blood sample combined with 1mL 1x RBC Lysis Buffer (eBiosciences) and incubated for 3min then quenched with PBS. RBC lysis was performed twice before proceeding to staining.

Human serum and plasma samples

De-identified human samples were used in this study with exempt IRB status granted from the Duke University Health System Institutional Review Board (protocol ID: Pro00112766). De-identified serum samples from 5 female and 5 male GBM patients were collected at time of recurrence and stored in vapor phase liquid nitrogen. These 10 samples are from the DERIVE and ELEVATE trials at Duke University (protocol IDs: Pro00054740 and Pro00082570). De-identified serum samples from 5 newly diagnosed GBM patients (3 males, 2 females) were collected at time of diagnosis and stored at -80°C. Newly diagnosed GBM patient samples were shared by Dr. Kyle Walsh at Duke University under the Preston Robert Tisch Brain Tumor Center Biorepository (protocol # Pro00007434, BTBR). De-identified healthy control human serum was purchased from BioIVT (5 males and 5 females, product # HUMANSRM-0001254 and HUMANSRM-0001253, respectively) and stored at -80°C until use. Given that these samples were not prospectively collected for our studies, we are unable to comment the specific collection methods for each individual sample.

Single-cell RNA sequencing analysis

Integration of a single cell atlas and downstream analyses were performed in Python (v3.9.13) using Scanpy (v1.9.1) and scvi-tools (v0.17.4). Filtered feature gene matrices from the following datasets were queried from the gene expression omnibus or provided by the original authors: GSE182109 (2 low grade glioma, 10 newly diagnosed GBM, 5 recurrent GBM)[103], GSE154795 (14 newly diagnosed GBM, 12 recurrent GBM, 5 PBMCs from recurrent GBM, 2 healthy donor PBMCs)[104], GSE160189 (5 normal brain)[105], GSE200218 (5 melanoma brain metastases)[106], and GSE186344 (3 breast cancer brain metastases, 3 lung cancer brain metastases, and 3 melanoma brain metastases)[107].

Matrices were read into Python with sc.read_10x_mtx(), and relevant metadata information was added (patient of origin, study of origin, tumor type). Anndata objects from each dataset were then concatenated with adata.concatenate() with join=outer. QC metrics were calculated and cells with >8000 genes by counts, <500 total counts, and >25 percent mitochondrial DNA were removed. A normalized counts layer for downstream analysis was created with sc.pp.normalize_total(), with a target sum of 10,000. 5000 highly variable genes were selected using scvi.data.poisson_gene_selection() with batch_key=patient of origin, and using the raw counts matrix, as is required for scvi. The model was then constructed using the filtered anndata object containing only highly variable genes with scvi.model.SCVI.setup_anndata(). Again, the

raw counts layer was used, with the batch_key set to patient of origin, and percent mitochondrial counts used as continuous categorical covariate. Because we were interested in primarily distinguishing between healthy cells, tumor cells, and immune cells, and not specific tumor types, tumor type was used as a categorical covariate in the model. The model was run with model.train() with an early stopping patience of 20 and 700 maximum epochs. The latent representation of the model was obtained with model.get_latent_representation() and added to .obsm of the original anndata object (containing all genes). For clustering, nearest neighbors were calculated using the .obsm latent representation from the model and n_neighbors=15, followed by sc.tl.umap() with min_dist=0.5 and sc.tl.leiden() with resolution=2.0. Clusters were analyzed individually with log1p total counts and percent mitochondrial counts. The model tends to cluster low quality cells (high mitochondrial content, high total counts, or low total counts) together, allowing for further quality control, rather than using a strict initial cutoff by QC metrics prior to visualizing data and cell types[108]. Expression of known marker genes from each tumor type, normal cell type, and immune cell components were evaluated by plotting gene expression onto the UMAP, using the normalized counts layer. We also assessed marker genes per leiden cluster with sc.tl.rank_genes_groups(), method=Wilcoxon, using the normalized counts layer. If a leiden cluster had exceptionally high or low total counts, or high mitochondrial counts, and did not align with known tumor, normal cell, or immune marker combinations (by UMAP gene expression and Wilcoxon Rank-Sum cluster markers), it was filtered out as low-quality cells or likely doublets. Each time leiden clusters were removed, another model was retrained with the same parameters, starting at the highly variable gene selection step and progressing through cluster quality control, until there were no clear low quality cell clusters remaining. Notably, in order to minimize bias in downstream analysis, expression of adrenergic receptors was not considered in any of the quality control and filtering steps.

All UMAP plots were generated with sc.pl.umap(), and clusters were annotated manually based on combinations of known marker genes. Matrix plots and Dot plots were generated with sc.pl.matrixplot() and sc.pl.dotplot(), respectively, with the normalized counts layer in both cases. For generating disease specific UMAPs, the global anndata object was subset based on patient metadata, and the primary UMAP embedding was retained to preserve graph architecture, allowing for easier comparison between subset and data objects.

In vivo Treatment

For immunotherapy administration, 200μg 4-1BB or vehicle control was administered intraperitoneally in 200μL PBS every 3 days, beginning at day 9, through day 18 post-tumor implantation for a total of 4 treatments.

For propranolol administration, mice were given 0.5g/L propranolol or vehicle control in drinking water *ad libitum* beginning on the day of tumor implantation.

For epinephrine/norepinephrine and salbutamol (beta-adrenergic receptor agonist) administration, naïve mice were implanted with subcutaneous osmotic pumps (Alzet) for seven days. Mice received a combination of 10mg/kg/day of epinephrine and 7mg/kg/day of norepinephrine or 8mg/kg/day of salbutamol.

Flow Cytometry

Cells were first washed with PBS then resuspended in Zombie Aqua Viability Dye (1:500 in PBS, Biolegend). For extracellular staining, samples were first resuspended in 50μL TruStain FcX Plus (1:500, Biolegend) in FACS buffer (2% FBS in PBS) for 15min at room temperature to block Fc receptors. After blocking, 50μL of a 2x antibody mastermix was added to samples and

samples were incubated for 30min at 4°C. Samples were then washed in FACs buffer and fixed with 2% formaldehyde in PBS for 20min at 4°C or fix/permeabilized for subsequent intracellular staining.

For intracellular staining, samples were fixed and permeabilized with a 1X FoxP3 Fixation/Permeabilization Buffer (eBioscience FoxP3/Transcription Factor Staining Buffer Set, Thermo Fisher Scientific) for 30min at 4°C.

Prior to sample acquisition, 10μL of Count Bright counting beads (Thermo Fisher Scientific) in 40μL of FACs buffer were added to each sample. Samples were acquired on a Fortessa (BD Biosciences) using FACS Diva software v.9 and analyzed using FlowJo v.10 (Tree Star).

Information regarding antibodies can be found below:

Marker	Color	Company	Catalog #	Clone
Live/Dead	BV510	Biolegend	423102	NA (Dye)
CD45	APC-Cy7	Biolegend	103116	30-F11
CD3	PE-Cy5	Biolegend	100310	145-2C11
CD19	PE-Cy5	Biolegend	115509	6D5
NK1.1	PE-Cy5	Biolegend	108715	PK136
Ly6G	PE-Cy5	Invitrogen	15-9668-82	1A8-Ly6g
CD64	BV711	Biolegend	139311	X54-5/7.1
CD11c	BV786	Biolegend	117335	N418
CD11b	PE	Biolegend	101207	M1/70
Siglec-H	PE-Cy7	Invitrogen	25-0333-80	eBio440c
MHCII	AF488	Biolegend	107615	M5/114.15.2
CD8	BV650	Biolegend	100742	53-6.7
CD103	PE-Dazzle	Biolegend	121429	2E7
XCR1	BV421	Biolegend	148216	ZET
CD40	BV605	BD Biosciences	745218	23-Mar
CD86	APC	Biolegend	105011	GL-1
CD3	PE	BD Biosciences	553064	145-2C11
CD4	BV605	Biolegend	100548	RM4-5
CD8	APCR700	BD Biosciences	564983	53-6.7
CD11b	PE Dazzle	BD Biosciences	562287	M1/70
Ly6C	BV650	Biolegend	128049	HK1.4
Ly6G	BV421	Biolegend	127627	1A8

F4/80	PE-Cy5	Biolegend	123112	BM8
MHCII	AF488	Biolegend	107615	M5/114.15.2
FoxP3	PE-Cy5.5	Biolegend	320012	150D
CD44	BV786	Biolegend	103059	N418
PD1	PE-Dazzle	Biolegend	109116	RMP1-30
CD25	BV421	Biolegend	102043	PC61
CD40L	PE-Cy7	Biolegend	106512	MR1
CD62L	PE-Cy5	Biolegend	104410	MEL-14
KLRG1	APC	Biolegend	138412	2F1/KLRG1
CD69	BV711	Biolegend	104537	H1.2F3
FoxP3	AF488	Biolegend	320012	150D

Single-Cell Cytokine Analysis

Spleens were harvested and T cells were isolated via untouched $CD8^+$ T cell isolation or Pan T cell isolation kits (Miltenyi) and stimulated ex vivo with plate-coated anti-CD3, soluble anti-CD28 antibodies (Invitrogen) for 16hours. T cells were then harvested and loaded into single-cell adaptive immune chips according to manufacturer instructions. Chips were run on the Isolight machine (Isoplexis) overnight and data were analyzed using IsoSpeak software (Isoplexis).

Gene Expression Analysis

C57BL/6 mice were implanted with intracranial CT2A glioma and treated with propranolol or vehicle control as described above. An additional non-tumor bearing group was included. Tumors were harvested and combined (n=5 tumors per group) with n=3 biological replicates per sample for a total of 15 tumors per sample. Immune cells were FACS-sorted for APC-enriched samples or T cell-enriched samples and RNA was subsequently extracted (RNeasy Mini Kit, Qiagen). RNA was analyzed on an nCounter MAX Analysis System (Nanostring) with the PanCancer Immune Profiling panel (Nanostring) according to manufacturer instructions. Expression data were analyzed using Rosalind, nSolver and nSolver Advanced Analysis software.

Human Retrospective Data

SEER is a population-based cancer registry that collects data on newly diagnosed cancers and provides cancer statistics for these cancers. SEER data are aggregated from cancer registries and contain patient demographic and tumor characteristics as well as the first course of treatment. SEER-Medicare[109,110] is the result of a linkage between existing SEER case data and detailed information about Medicare beneficiary's covered healthcare services from the time of Medicare eligibility until death. The linked dataset includes 15 SEER registries covering ~24% of the US population. Medicare included approximately 95% of patients age 65 and older in the SEER files[110]. Additionally, among all Medicare enrollees, the proportion of those enrolled in Medicare Advantage plans has increased from 21% in 2008 to 34% in 2018.[111] As enrollees in Advantage plans will lack claims for the time period they are enrolled, this restriction represents a significant limitation to the population that is able to be used. Furthermore, as some patients may have private health insurance or not be continuously enrolled in Medicare Part B in addition to Part A, there is a possibility that some included individuals may have an incomplete claims history.

Cases of primary GBM (International Classification of Diseases for Oncology 3rd Edition (ICD-O-3)[112] morphology codes 9440/3, 9441/3, 9442/3, 9445/3; topographic codes C71.0-C71.9), melanoma (ICD-O-3 morphology codes 8720/3-8790/3, ICD-O-3 topographic codes C44.0-C44.9) and lung cancer (ICD-O-3 morphology codes 8000/3-8579/3, ICD-O-3 topographic codes C34.0-C34.9) were identified in the SEER cancer file for diagnoses made from January 1, 2008 – December 1, 2017, excluding patients younger than 65 years and those enrolled due to end-stage renal disease or disability **(ICD codes in Supplementary Table 1**). Patients enrolled in a Health Maintenance Organization six months prior and twelve months after primary diagnosis were excluded (34.1% of lung cancer, 31.3% of melanoma, 24.3% of glioblastoma), in addition to those enrolled in Medicare Part D. Additionally, those with a prior cancer diagnosis, which was identified using a SEER-provided variable (*Sequence_number)*, were also excluded (36.9% of lung cancer, 53.9% of melanoma, 32.8% of glioblastoma). Finally, observations with missing age, race, ethnicity, sex, and survival or follow-up time were excluded from the analysis.

Intracranial metastases were identified using the SEER synchronous brain metastasis variable and the Medicare Provider Analysis and Review (MEDPAR), National Claims History (NCH), and Outpatient (OUTPAT) claims files. Patients with intracranial metastases were defined as those with a diagnosis code for an intracranial metastasis (International Classification of Diseases 9th and 10th Ed. (ICD-9 and ICD-10) codes 198.3 and C79.3, respectively) and at least one procedure code for a brain or head diagnostic test within 60 days of the intracranial metastasis diagnosis (Current Procedural Terminology[113] codes 70450-70470, 70551-70553, 78607-78608). Prior comorbidity score was estimated using the rule-out option of the SEER-Medicare SAS comorbidity macro (2021 version)[114] using both ICD-9 and ICD-10 diagnosis codes. The comorbidity scores were calculated with Charlson weights and grouped as a score of 0, 1, 2, and 3+. Cancer treatment patterns – including radiation, chemotherapy, β-blocker, and checkpoint blockade usage (including Pembrolizumab, Necitumumab, Nivolumab, Ipilimumab, Atezolizumab, and Ramucirumab) – were identified using both SEER data and the MEDPAR, NCH, OUTPAT, Part D Event, and Durable Medical Equipment files. Surgery was identified using SEER -provided variable (*RX_Summ_Surg_prim-Site_1998)* which includes biopsies with excision and claims with CPT and ICD codes specific to the type of primary cancer (Supplementary table 1). Radiation therapy and chemotherapy were defined by ≥2 claims for the same code separated by at least one week, and prior use of β-blockers was defined as ≥2 dispensing for the same β-blocker prior to diagnosis (Supplementary table 1). Patients that started checkpoint blockade before detection of intracranial metastasis were excluded from the analysis.

Kaplan-Meier estimation was used to assess the effect of a combination β-blocker and checkpoint blockade versus checkpoint blockade alone on overall survival. In GBM, where no checkpoint inhibitors are currently approved for use, the effect of β-blockers on overall survival was examined. Cox proportional hazards models were used to assess the relationship between combination β-blocker and checkpoint blockade versus checkpoint blockade alone among the cohorts, adjusting for SEER-provided demographics – including age, sex (male or female), and race/ethnicity (non-Hispanic White, non-Hispanic Black, non-Hispanic Other, or Hispanic [all races], or Unknown) – treatment patterns (yes/no surgery, radiation and chemotherapy), and prior comorbidity score.

Analyses were performed overall by cancer type. Statistical significance was assessed at alpha level 0.05. All analyses were conducted using R version 4.1.3 using the following packages: gtsummary, patchwork, survival, survminer, and tidyverse suite.[115-119]

Statistical Analyses

Experimental group assignment was determined by random designation. All measurements were taken from distinct samples. The statistical tests employed for each data presentation and number of samples (n) are designated in the respective figure legends. Individual data points are represented as dots in graphs. Statistical analyses were performed using GraphPad Prism software. Error bars represent the standard error of the mean (SEM). No data were excluded from analysis. Mice were randomized into treatment groups after tumor injection. P-values <0.05 were considered statistically significant. Investigators were not blinded to group assignment during experimental procedures or analysis, but survival studies were monitored both by investigators and additionally monitored by veterinary staff form the Duke animal facility who were blinded to the studies and reported humane endpoints accordingly.

Ethics statement

All studies performed in research animals and on clinical samples are compliant with all relevant ethical regulations. All animal experiments were approved by the IACUC at Duke University Medical Center (protocol A163-21-08). De-identified human samples were used in this study with exempt IRB status granted from the Duke University Health System Institutional Review Board (protocol ID: Pro00112766).

DATA AVAILABILITY

All scRNAseq datasets used for analysis are publicly available: GSE182109[103], GSE154795[104], GSE160189[105], GSE200218[106], and GSE186344[107]. SEER-Medicare data are publicly available, but these data are released on a project-specific basis that requires an approved application. Applications are reviewed by NCI-led content experts and application revisions may be required. Initial reviewer comments are typically provided within 2-3 weeks. Fees are incurred to cover the cost of creating the requested data files. Instructions for the application can be found here: https://healthcaredelivery.cancer.gov/seermedicare/obtain/requests.html#docs. Gene expression data that support the findings of this study have been deposited in the Gene Expression Omnibus under the accession number GSE241720.

CODE AVAILABILITY

Integration and analysis of publicly available scRNAseq datasets were conducted based on publicly available workflows and can be accessed at https://github.com/jbfinlay/Lorrey_Wachsmuth_et_al. Analysis of relevant SEER-Medicare data can be accessed at https://zenodo.org/record/8289570.

REFERENCES

1 Reardon, D. A. *et al.* Effect of Nivolumab vs Bevacizumab in Patients With Recurrent Glioblastoma: The CheckMate 143 Phase 3 Randomized Clinical Trial. *JAMA Oncol* **6**, 1003-1010, doi:10.1001/jamaoncol.2020.1024 (2020).

2 Lim, M. *et al.* Phase III trial of chemoradiotherapy with temozolomide plus nivolumab or placebo for newly diagnosed glioblastoma with methylated MGMT promoter. *Neuro Oncol* **24**, 1935-1949, doi:10.1093/neuonc/noac116 (2022).

3 Omuro, A. *et al.* Radiotherapy combined with nivolumab or temozolomide for newly diagnosed glioblastoma with unmethylated MGMT promoter: An international randomized phase III trial. *Neuro Oncol* **25**, 123-134, doi:10.1093/neuonc/noac099 (2023).

4 Woroniecka, K. I., Rhodin, K. E., Chongsathidkiet, P., Keith, K. A. & Fecci, P. E. T-cell Dysfunction in Glioblastoma: Applying a New Framework. *Clin Cancer Res* **24**, 3792-3802, doi:10.1158/1078-0432.ccr-18-0047 (2018).

5 Brooks, W. H., Caldwell, H. D. & Mortara, R. H. Immune responses in patients with gliomas. *Surg Neurol* **2**, 419-423 (1974).

6 Brooks, W. H., Netsky, M. G., Normansell, D. E. & Horwitz, D. A. Depressed cell-mediated immunity in patients with primary intracranial tumors. Characterization of a humoral immunosuppressive factor. *J Exp Med* **136**, 1631-1647 (1972).

7 Brooks, W. H., Roszman, T. L., Mahaley, M. S. & Woosley, R. E. Immunobiology of primary intracranial tumours. II. Analysis of lymphocyte subpopulations in patients with primary brain tumours. *Clin Exp Immunol* **29**, 61-66 (1977).

8 Brooks, W. H., Roszman, T. L. & Rogers, A. S. Impairment of rosette-forming T lymphoctyes in patients with primary intracranial tumors. *Cancer* **37**, 1869-1873 (1976).

9 Dix, A. R., Brooks, W. H., Roszman, T. L. & Morford, L. A. Immune defects observed in patients with primary malignant brain tumors. *J Neuroimmunol* **100**, 216-232 (1999).

10 Elliott, L., Brooks, W. & Roszman, T. Role of interleukin-2 (IL-2) and IL-2 receptor expression in the proliferative defect observed in mitogen-stimulated lymphocytes from patients with gliomas. *Journal of the National Cancer Institute* **78**, 919-922 (1987).

11 Elliott, L. H., Brooks, W. H. & Roszman, T. L. Cytokinetic basis for the impaired activation of lymphocytes from patients with primary intracranial tumors. *Journal of Immunology* **132**, 1208-1215 (1984).

12 Elliott, L. H., Brooks, W. H. & Roszman, T. L. Inability of mitogen-activated lymphocytes obtained from patients with malignant primary intracranial tumors to express high affinity interleukin 2 receptors. *Journal of Clinical Investigation* **86**, 80-86 (1990).

13 Mahaley, M. S., Jr. *et al.* Immunobiology of primary intracranial tumors. Part 1: studies of the cellular and humoral general immune competence of brain-tumor patients. *Journal of Neurosurgery* **46**, 467-476 (1977).

14 McVicar, D. W., Davis, D. F. & Merchant, R. E. In vitro analysis of the proliferative potential of T cells from patients with brain tumor: glioma-associated immunosuppression unrelated to intrinsic cellular defect. *Journal of Neurosurgery* **76**, 251-260 (1992).

15 Morford, L. A., Elliott, L. H., Carlson, S. L., Brooks, W. H. & Roszman, T. L. T cell receptor-mediated signaling is defective in T cells obtained from patients with primary intracranial tumors. *Journal of Immunology* **159**, 4415-4425 (1997).

16 Roszman, T. L. & Brooks, W. H. Immunobiology of primary intracranial tumours. III. Demonstration of a qualitative lymphocyte abnormality in patients with primary brain tumours. *Clin Exp Immunol* **39**, 395-402 (1980).

17 Roszman, T. L., Brooks, W. H. & Elliott, L. H. Immunobiology of primary intracranial tumors. VI. Suppressor cell function and lectin-binding lymphocyte subpopulations in patients with cerebral tumors. *Cancer* **50**, 1273-1279 (1982).

18 Roszman, T. L., Brooks, W. H. & Elliott, L. H. Inhibition of lymphocyte responsiveness by a glial tumor cell-derived suppressive factor. *Journal of Neurosurgery* **67**, 874-879 (1987).

19 Young, H. F., Sakalas, R. & Kaplan, A. M. Inhibition of cell-mediated immunity in patients with brain tumors. *Surg Neurol* **5**, 19-23 (1976).

20 Chongsathidkiet, P. *et al.* Sequestration of T cells in bone marrow in the setting of glioblastoma and other intracranial tumors. *Nat Med* **24**, 1459-1468, doi:10.1038/s41591-018-0135-2 (2018).

21 Dunn, G. P., Fecci, P. E. & Curry, W. T. Cancer immunoediting in malignant glioma. *Neurosurgery* **71**, 201-223 (2012).

22 Fecci, P. E., Heimberger, A. B. & Sampson, J. H. Immunotherapy for primary brain tumors: no longer a matter of privilege. *Clin Cancer Res* **20**, 5620-5629, doi:10.1158/1078-0432.CCR-14-0832 (2014).

23 Fecci, P. E. & Sampson, J. H. The current state of immunotherapy for gliomas: an eye toward the future. *J Neurosurg* **131**, 657-666, doi:10.3171/2019.5.Jns181762 (2019).

24 Grabowski, M. M. *et al.* Immune suppression in gliomas. *J Neurooncol* **151**, 3-12, doi:10.1007/s11060-020-03483-y (2021).

25 Miggelbrink, A. M. *et al.* CD4 T-Cell Exhaustion: Does It Exist and What Are Its Roles in Cancer? *Clin Cancer Res* **27**, 5742-5752, doi:10.1158/1078-0432.CCR-21-0206 (2021).

26 Sampson, J. H., Gunn, M. D., Fecci, P. E. & Ashley, D. M. Brain immunology and immunotherapy in brain tumours. *Nature reviews. Cancer* **20**, 12-25, doi:10.1038/s41568-019-0224-7 (2020).

27 Woroniecka, K. *et al.* T Cell Exhaustion Signatures Vary with Tumor Type and are Severe in Glioblastoma. *Clin Cancer Res*, doi:10.1158/1078-0432.ccr-17-1846 (2018).

28 Fecci, P. E. *et al.* Systemic CTLA-4 blockade ameliorates glioma-induced changes to the CD4+ T cell compartment without affecting regulatory T-cell function. *Clin Cancer Res* **13**, 2158-2167, doi:13/7/2158 [pii]
10.1158/1078-0432.CCR-06-2070 (2007).

29 Kizaki, T. *et al.* Beta2-adrenergic receptor regulates Toll-like receptor-4-induced nuclear factor-kappaB activation through beta-arrestin 2. *Immunology* **124**, 348-356, doi:10.1111/j.1365-2567.2007.02781.x (2008).

30 Safi, S. Z. *et al.* Beta Adrenergic Receptors Stimulation Attenuates Phosphorylation of NF-kappaB and IkappaBalpha in Hyperglycemic Endothelial Cells. *Cell Physiol Biochem* **51**, 1429-1436, doi:10.1159/000495591 (2018).

31 Takenaka, M. C. *et al.* Norepinephrine Controls Effector T Cell Differentiation through beta2-Adrenergic Receptor-Mediated Inhibition of NF-kappaB and AP-1 in Dendritic Cells. *J Immunol* **196**, 637-644, doi:10.4049/jimmunol.1501206 (2016).

32 Farmer, P. & Pugin, J. beta-adrenergic agonists exert their "anti-inflammatory" effects in monocytic cells through the IkappaB/NF-kappaB pathway. *Am J Physiol Lung Cell Mol Physiol* **279**, L675-682, doi:10.1152/ajplung.2000.279.4.L675 (2000).

33 Verhoeckx, K. C., Doornbos, R. P., van der Greef, J., Witkamp, R. F. & Rodenburg, R. J. Inhibitory effects of the beta-adrenergic receptor agonist zilpaterol on the LPS-induced production of TNF-alpha in vitro and in vivo. *J Vet Pharmacol Ther* **28**, 531-537, doi:10.1111/j.1365-2885.2005.00691.x (2005).

34 Izeboud, C. A., Monshouwer, M., van Miert, A. S. & Witkamp, R. F. The beta-adrenoceptor agonist clenbuterol is a potent inhibitor of the LPS-induced production of TNF-alpha and IL-6 in vitro and in vivo. *Inflamm Res* **48**, 497-502, doi:10.1007/s000110050493 (1999).

35 Ausiello, C. M. *et al.* Cell mediated cytotoxicity and cytokine production in peripheral blood mononuclear cells of glioma patients. *European Journal of Cancer* **27**, 646-650 (1991).

36 Dunn, G. P., Fecci, P. E. & Curry, W. T. Cancer immunoediting in malignant glioma. *Neurosurgery* **71**, 201-222; discussion 222-203, doi:10.1227/NEU.0b013e31824f840d (2012).

37 Morford, L. A., Dix, A. R., Brooks, W. H. & Roszman, T. L. Apoptotic elimination of peripheral T lymphocytes in patients with primary intracranial tumors. *Journal of Neurosurgery* **91**, 935-946 (1999).

38 Roussel, E., Gingras, M. C., Grimm, E. A., Bruner, J. M. & Moser, R. P. Predominance of a type 2 intratumoural immune response in fresh tumour-infiltrating lymphocytes from human gliomas. *Clin Exp Immunol* **105**, 344-352 (1996).

39 Young, H. F. & Kaplan, A. M. Cellular immune deficiency in patients with glioblastoma. *Surg Forum* **27**, 476-478 (1976).

40 Young, H. F., Sakalas, R. & Kaplan, A. M. Immunologic depression in cerebral gliomas. *Adv Neurol* **15**, 327-335 (1976).

41 Fecci, P. E. *et al.* Increased regulatory T-cell fraction amidst a diminished CD4 compartment explains cellular immune defects in patients with malignant glioma. *Cancer Res* **66**, 3294-3302, doi:10.1158/0008-5472.CAN-05-3773 (2006).

42 Reap, E. A. *et al.* Dendritic Cells Enhance Polyfunctionality of Adoptively Transferred T Cells That Target Cytomegalovirus in Glioblastoma. *Cancer Res* **78**, 256-264, doi:10.1158/0008-5472.can-17-0469 (2018).

43 Huff, W. X. *et al.* Aging- and Tumor-Mediated Increase in CD8(+)CD28(-) T Cells Might Impose a Strong Barrier to Success of Immunotherapy in Glioblastoma. *Immunohorizons* **5**, 395-409, doi:10.4049/immunohorizons.2100008 (2021).

44 Thibaudin, M. *et al.* Targeting PD-L1 and TIGIT could restore intratumoral CD8 T cell function in human colorectal cancer. *Cancer Immunol Immunother* **71**, 2549-2563, doi:10.1007/s00262-022-03182-9 (2022).

45 Miller, B. C. *et al.* Subsets of exhausted CD8(+) T cells differentially mediate tumor control and respond to checkpoint blockade. *Nat Immunol* **20**, 326-336, doi:10.1038/s41590-019-0312-6 (2019).

46 Ma, L. *et al.* Enhanced CAR-T cell activity against solid tumors by vaccine boosting through the chimeric receptor. *Science* **365**, 162-168, doi:10.1126/science.aav8692 (2019).

47 Sarkar, S. *et al.* Programming of CD8 T Cell Quantity and Polyfunctionality by Direct IL-1 Signals. *J Immunol* **201**, 3641-3650, doi:10.4049/jimmunol.1800906 (2018).

48 Zurko, J. C. *et al.* Bispecific targeting of CD20 and CD19 increases polyfunctionality of chimeric antigen receptor T-cell products in B-cell malignancies. *Cytotherapy* **24**, 767-773, doi:10.1016/j.jcyt.2022.03.011 (2022).

49 Yoshikawa, T. *et al.* Genetic ablation of PRDM1 in antitumor T cells enhances therapeutic efficacy of adoptive immunotherapy. *Blood* **139**, 2156-2172, doi:10.1182/blood.2021012714 (2022).

50 Sung, B. Y. *et al.* Wnt activation promotes memory T cell polyfunctionality via epigenetic regulator PRMT1. *J Clin Invest* **132**, doi:10.1172/JCI140508 (2022).

51 Doescher, J. *et al.* Polyfunctionality of CD4(+) T lymphocytes is increased after chemoradiotherapy of head and neck squamous cell carcinoma. *Strahlenther Onkol* **194**, 392-402, doi:10.1007/s00066-018-1289-z (2018).

52 Kaptein, P. *et al.* Addition of interleukin-2 overcomes resistance to neoadjuvant CTLA4 and PD1 blockade in ex vivo patient tumors. *Sci Transl Med* **14**, eabj9779, doi:10.1126/scitranslmed.abj9779 (2022).

53 Migueles, S. A. *et al.* Defective human immunodeficiency virus-specific CD8+ T-cell polyfunctionality, proliferation, and cytotoxicity are not restored by antiretroviral therapy. *J Virol* **83**, 11876-11889, doi:10.1128/JVI.01153-09 (2009).
54 Egelston, C. A. *et al.* Human breast tumor-infiltrating CD8(+) T cells retain polyfunctionality despite PD-1 expression. *Nat Commun* **9**, 4297, doi:10.1038/s41467-018-06653-9 (2018).
55 Ramello, M. C. *et al.* Polyfunctional KLRG-1(+)CD57(+) Senescent CD4(+) T Cells Infiltrate Tumors and Are Expanded in Peripheral Blood From Breast Cancer Patients. *Front Immunol* **12**, 713132, doi:10.3389/fimmu.2021.713132 (2021).
56 Rossi, J. *et al.* Preinfusion polyfunctional anti-CD19 chimeric antigen receptor T cells are associated with clinical outcomes in NHL. *Blood* **132**, 804-814, doi:10.1182/blood-2018-01-828343 (2018).
57 Waterhouse, N. J., Sedelies, K. A. & Clarke, C. J. Granzyme B; the chalk-mark of a cytotoxic lymphocyte. *J Transl Med* **2**, 36, doi:10.1186/1479-5876-2-36 (2004).
58 Heusel, J. W., Wesselschmidt, R. L., Shresta, S., Russell, J. H. & Ley, T. J. Cytotoxic lymphocytes require granzyme B for the rapid induction of DNA fragmentation and apoptosis in allogeneic target cells. *Cell* **76**, 977-987, doi:10.1016/0092-8674(94)90376-x (1994).
59 Wang, H. *et al.* beta-arrestin2 functions as a key regulator in the sympathetic-triggered immunodepression after stroke. *J Neuroinflammation* **15**, 102, doi:10.1186/s12974-018-1142-4 (2018).
60 Watowich, M. B., Gilbert, M. R. & Larion, M. T cell exhaustion in malignant gliomas. *Trends Cancer* **9**, 270-292, doi:10.1016/j.trecan.2022.12.008 (2023).
61 Woroniecka, K. & Fecci, P. E. T-cell exhaustion in glioblastoma. *Oncotarget* **9**, 35287-35288, doi:10.18632/oncotarget.26228 (2018).
62 Liu, T., Zhang, L., Joo, D. & Sun, S. C. NF-kappaB signaling in inflammation. *Signal Transduct Target Ther* **2**, 17023-, doi:10.1038/sigtrans.2017.23 (2017).
63 Barnes, S. E. *et al.* T cell-NF-kappaB activation is required for tumor control in vivo. *J Immunother Cancer* **3**, 1, doi:10.1186/s40425-014-0045-x (2015).
64 Bottcher, J. P. & Reis e Sousa, C. The Role of Type 1 Conventional Dendritic Cells in Cancer Immunity. *Trends Cancer* **4**, 784-792, doi:10.1016/j.trecan.2018.09.001 (2018).
65 Cancel, J. C., Crozat, K., Dalod, M. & Mattiuz, R. Are Conventional Type 1 Dendritic Cells Critical for Protective Antitumor Immunity and How? *Front Immunol* **10**, 9, doi:10.3389/fimmu.2019.00009 (2019).
66 Marigo, I. *et al.* T Cell Cancer Therapy Requires CD40-CD40L Activation of Tumor Necrosis Factor and Inducible Nitric-Oxide-Synthase-Producing Dendritic Cells. *Cancer Cell* **30**, 651, doi:10.1016/j.ccell.2016.09.009 (2016).
67 Frentsch, M. *et al.* CD40L expression permits CD8+ T cells to execute immunologic helper functions. *Blood* **122**, 405-412, doi:10.1182/blood-2013-02-483586 (2013).
68 Razavi, S. M. *et al.* Immune Evasion Strategies of Glioblastoma. *Front Surg* **3**, 11, doi:10.3389/fsurg.2016.00011 (2016).
69 Rui, Y. & Green, J. J. Overcoming delivery barriers in immunotherapy for glioblastoma. *Drug Deliv Transl Res* **11**, 2302-2316, doi:10.1007/s13346-021-01008-2 (2021).
70 Bausart, M., Preat, V. & Malfanti, A. Immunotherapy for glioblastoma: the promise of combination strategies. *J Exp Clin Cancer Res* **41**, 35, doi:10.1186/s13046-022-02251-2 (2022).
71 Himes, B. T. *et al.* Immunosuppression in Glioblastoma: Current Understanding and Therapeutic Implications. *Front Oncol* **11**, 770561, doi:10.3389/fonc.2021.770561 (2021).
72 Bucsek, M. J., Giridharan, T., MacDonald, C. R., Hylander, B. L. & Repasky, E. A. An overview of the role of sympathetic regulation of immune responses in infectious disease

and autoimmunity. *Int J Hyperthermia* **34**, 135-143, doi:10.1080/02656736.2017.1411621 (2018).

73 Westendorp, W. F., Nederkoorn, P. J., Vermeij, J. D., Dijkgraaf, M. G. & van de Beek, D. Post-stroke infection: a systematic review and meta-analysis. *BMC Neurol* **11**, 110, doi:10.1186/1471-2377-11-110 (2011).

74 Deng, Q. W. *et al.* Blocking Sympathetic Nervous System Reverses Partially Stroke-Induced Immunosuppression but does not Aggravate Functional Outcome After Experimental Stroke in Rats. *Neurochem Res* **41**, 1877-1886, doi:10.1007/s11064-016-1899-8 (2016).

75 Bullock, T. N. J. CD40 stimulation as a molecular adjuvant for cancer vaccines and other immunotherapies. *Cell Mol Immunol* **19**, 14-22, doi:10.1038/s41423-021-00734-4 (2022).

76 Ferris, S. T. *et al.* cDC1 prime and are licensed by CD4(+) T cells to induce anti-tumour immunity. *Nature* **584**, 624-629, doi:10.1038/s41586-020-2611-3 (2020).

77 Wu, R. *et al.* Mechanisms of CD40-dependent cDC1 licensing beyond costimulation. *Nat Immunol* **23**, 1536-1550, doi:10.1038/s41590-022-01324-w (2022).

78 Broz, M. L. *et al.* Dissecting the Tumor Myeloid Compartment Reveals Rare Activating Antigen-Presenting Cells Critical for T Cell Immunity. *Cancer Cell* **26**, 938, doi:10.1016/j.ccell.2014.11.010 (2014).

79 Bottcher, J. P. *et al.* NK Cells Stimulate Recruitment of cDC1 into the Tumor Microenvironment Promoting Cancer Immune Control. *Cell* **172**, 1022-1037 e1014, doi:10.1016/j.cell.2018.01.004 (2018).

80 Salmon, H. *et al.* Expansion and Activation of CD103(+) Dendritic Cell Progenitors at the Tumor Site Enhances Tumor Responses to Therapeutic PD-L1 and BRAF Inhibition. *Immunity* **44**, 924-938, doi:10.1016/j.immuni.2016.03.012 (2016).

81 Spranger, S., Dai, D., Horton, B. & Gajewski, T. F. Tumor-Residing Batf3 Dendritic Cells Are Required for Effector T Cell Trafficking and Adoptive T Cell Therapy. *Cancer Cell* **31**, 711-723 e714, doi:10.1016/j.ccell.2017.04.003 (2017).

82 Chonan, M. *et al.* CD40/CD40L expression correlates with the survival of patients with glioblastomas and an augmentation in CD40 signaling enhances the efficacy of vaccinations against glioma models. *Neuro Oncol* **17**, 1453-1462, doi:10.1093/neuonc/nov090 (2015).

83 Kim, H. S. *et al.* Propranolol Inhibits the Proliferation of Human Glioblastoma Cell Lines through Notch1 and Hes1 Signaling System. *J Korean Neurosurg Soc* **64**, 716-725, doi:10.3340/jkns.2021.0068 (2021).

84 Tewarie, I. A., Senders, J. T., Hulsbergen, A. F. C., Kremer, S. & Broekman, M. L. D. Beta-blockers and glioma: a systematic review of preclinical studies and clinical results. *Neurosurg Rev* **44**, 669-677, doi:10.1007/s10143-020-01277-4 (2021).

85 Prados, M. D. *et al.* Toward precision medicine in glioblastoma: the promise and the challenges. *Neuro Oncol* **17**, 1051-1063, doi:10.1093/neuonc/nov031 (2015).

86 Wang, X. *et al.* Norepinephrine promotes glioma cell migration through up-regulating the expression of Twist1. *BMC cancer* **22**, 213, doi:10.1186/s12885-022-09330-9 (2022).

87 Johansen, M. D. *et al.* Outcome of Bevacizumab Therapy in Patients with Recurrent Glioblastoma Treated with Angiotensin System Inhibitors. *Cancer Invest* **36**, 512-519, doi:10.1080/07357907.2018.1544639 (2018).

88 De Giorgi, V. *et al.* Effect of beta-blockers and other antihypertensive drugs on the risk of melanoma recurrence and death. *Mayo Clin Proc* **88**, 1196-1203, doi:10.1016/j.mayocp.2013.09.001 (2013).

89 De Giorgi, V. *et al.* Propranolol for Off-label Treatment of Patients With Melanoma: Results From a Cohort Study. *JAMA Oncol* **4**, e172908, doi:10.1001/jamaoncol.2017.2908 (2018).

90 McCourt, C. *et al.* Beta-blocker usage after malignant melanoma diagnosis and survival: a population-based nested case-control study. *Br J Dermatol* **170**, 930-938, doi:10.1111/bjd.12894 (2014).
91 Katsarelias, D. *et al.* The Effect of Beta-Adrenergic Blocking Agents in Cutaneous Melanoma-A Nation-Wide Swedish Population-Based Retrospective Register Study. *Cancers (Basel)* **12**, doi:10.3390/cancers12113228 (2020).
92 Gandhi, S. *et al.* Phase I Clinical Trial of Combination Propranolol and Pembrolizumab in Locally Advanced and Metastatic Melanoma: Safety, Tolerability, and Preliminary Evidence of Antitumor Activity. *Clin Cancer Res* **27**, 87-95, doi:10.1158/1078-0432.CCR-20-2381 (2021).
93 Calvani, M. *et al.* Norepinephrine promotes tumor microenvironment reactivity through beta3-adrenoreceptors during melanoma progression. *Oncotarget* **6**, 4615-4632, doi:10.18632/oncotarget.2652 (2015).
94 Eng, J. W. *et al.* A nervous tumor microenvironment: the impact of adrenergic stress on cancer cells, immunosuppression, and immunotherapeutic response. *Cancer Immunol Immunother* **63**, 1115-1128, doi:10.1007/s00262-014-1617-9 (2014).
95 Wrobel, L. J., Gayet-Ageron, A. & Le Gal, F. A. Effects of Beta-Blockers on Melanoma Microenvironment and Disease Survival in Human. *Cancers (Basel)* **12**, doi:10.3390/cancers12051094 (2020).
96 Jean Wrobel, L. *et al.* Propranolol induces a favourable shift of anti-tumor immunity in a murine spontaneous model of melanoma. *Oncotarget* **7**, 77825-77837, doi:10.18632/oncotarget.12833 (2016).
97 Fjaestad, K. Y. *et al.* Blockade of beta-adrenergic receptors reduces cancer growth and enhances the response to anti-CTLA4 therapy by modulating the tumor microenvironment. *Oncogene* **41**, 1364-1375, doi:10.1038/s41388-021-02170-0 (2022).
98 Ashrafi, S., Shapouri, R., Shirkhani, A. & Mahdavi, M. Anti-tumor effects of propranolol: Adjuvant activity on a transplanted murine breast cancer model. *Biomed Pharmacother* **104**, 45-51, doi:10.1016/j.biopha.2018.05.002 (2018).
99 Kokolus, K. M. *et al.* Beta blocker use correlates with better overall survival in metastatic melanoma patients and improves the efficacy of immunotherapies in mice. *Oncoimmunology* **7**, e1405205, doi:10.1080/2162402X.2017.1405205 (2018).
100 Ostrom, Q. T., Wright, C. H. & Barnholtz-Sloan, J. S. Brain metastases: epidemiology. *Handb Clin Neurol* **149**, 27-42, doi:10.1016/B978-0-12-811161-1.00002-5 (2018).
101 Barnholtz-Sloan, J. S. *et al.* Incidence proportions of brain metastases in patients diagnosed (1973 to 2001) in the Metropolitan Detroit Cancer Surveillance System. *J Clin Oncol* **22**, 2865-2872, doi:10.1200/JCO.2004.12.149 (2004).
102 Srinivasan, A. V. Propranolol: A 50-Year Historical Perspective. *Ann Indian Acad Neurol* **22**, 21-26, doi:10.4103/aian.AIAN_201_18 (2019).
103 Abdelfattah, N. *et al.* Single-cell analysis of human glioma and immune cells identifies S100A4 as an immunotherapy target. *Nat Commun* **13**, 767, doi:10.1038/s41467-022-28372-y (2022).
104 Lee, A. H. *et al.* Neoadjuvant PD-1 blockade induces T cell and cDC1 activation but fails to overcome the immunosuppressive tumor associated macrophages in recurrent glioblastoma. *Nat Commun* **12**, 6938, doi:10.1038/s41467-021-26940-2 (2021).
105 Ayhan, F. *et al.* Resolving cellular and molecular diversity along the hippocampal anterior-to-posterior axis in humans. *Neuron* **109**, 2091-2105 e2096, doi:10.1016/j.neuron.2021.05.003 (2021).
106 Biermann, J. *et al.* Dissecting the treatment-naive ecosystem of human melanoma brain metastasis. *Cell* **185**, 2591-2608 e2530, doi:10.1016/j.cell.2022.06.007 (2022).
107 Gonzalez, H. *et al.* Cellular architecture of human brain metastases. *Cell* **185**, 729-745 e720, doi:10.1016/j.cell.2021.12.043 (2022).

108 Heumos, L. *et al.* Best practices for single-cell analysis across modalities. *Nat Rev Genet* **24**, 550-572, doi:10.1038/s41576-023-00586-w (2023).
109 Enewold, L. *et al.* Updated Overview of the SEER-Medicare Data: Enhanced Content and Applications. *J Natl Cancer Inst Monogr* **2020**, 3-13, doi:10.1093/jncimonographs/lgz029 (2020).
110 (ed National Cancer Institute) (2022).
111 Neuman, P. & Jacobson, G. A. Medicare Advantage Checkup. *New England Journal of Medicine* **379**, 2163-2172, doi:10.1056/NEJMhpr1804089 (2018).
112 Fritz A, P. C., Jack A, Shanmugaratnam K, Sobin L, Perkin DM, Whelan S (World Health Organization, 2000).
113 Dotson, P. CPT(®) Codes: What Are They, Why Are They Necessary, and How Are They Developed? *Adv Wound Care (New Rochelle)* **2**, 583-587, doi:10.1089/wound.2013.0483 (2013).
114 Program, H. D. R. *Comorbidity SAS Macro (2021 version)*, <https://healthcaredelivery.cancer.gov/seermedicare/considerations/macro-2021.html> (2021).
115 Daniel D. Sjoberg, K. W., Michael Curry, Jessica A. Lavery and Joseph Larmarange. Reproducible Summary Tables with the gtsummary Package. *The R Journal* **13**, 570-580 (2021).
116 Thomas Lin Pedersen v. R package version 1.1.1 (2020).
117 Terry M. Therneau, P. M. G. *A Package for Survival Analysis in R.* R package version 3.2-11 edn, (2021).
118 survminer: Drawing Survival Curves using 'ggplot2'. v. R package version 0.4.9. (2021).
119 Wickham, H. A., M; Bryan, J et al. . Welcome to the tidyverse. *Journal of Open Source Software* **4**, 1686, doi:https://doi.org/10.21105/joss.01686 (2019).

Table 1. Inclusion and Exclusion Criteria for Retrospective Analysis of Patients with Glioblastoma or Melanoma Intracranial Metastasis or Lung Cancer Intracranial Metastasis

Inclusion and Exclusion Criteria		
Glioblastoma	**Melanoma**	**Lung Cancer**
Included: GBM at primary site C71.0-C71.9, morphology code 9440/3-9445/3	**Included:** patients with melanoma at primary site C44.0-44.9, morphology code 8720/3-8790/3	**Included:** patients with lung cancer at primary site C34.0-34.9, morphology code 8000/3-8579/3
Excluded: patients ages < 65 years	**Excluded:** patients ages <65 years	**Excluded:** patients ages <65 years
Excluded: patients enrolled due to ESRD	**Excluded:** patients enrolled due to ESRD	**Excluded:** patients enrolled due to ESRD
Excluded: patients enrolled in an HMO 6 months prior to 12 months following diagnosis	**Excluded:** patients enrolled in an HMO 6 months prior to 12 months following diagnosis	**Excluded:** patients enrolled in an HMO 6 months prior to 12 months following diagnosis
Excluded: patients those with prior cancer diagnosis	**Excluded:** patients with prior cancer diagnosis	**Excluded:** patients with prior cancer diagnosis
Excluded: patients missing age of diagnosis, sex, race, or follow-up time	**Excluded:** patients with missing age of diagnosis, sex, race, or follow-up time	**Excluded:** patients with missing age of diagnosis, sex, race, or follow-up time
	Excluded: patients with a history of checkpoint inhibitor use before diagnosis with brain metastasis	**Excluded:** patients with a history of checkpoint inhibitor use before diagnosis with brain metastasis

Table 2. Demographic Characteristics of Glioblastoma, Lung Cancer, and Melanoma Cases by Metastases in SEER-Medicare, 2008-2017

	Glioblastoma	*Lung Cancer*	*Melanoma*
Characteristic	**Overall, N = 8,743**	**Any intracranial metastasis N = 1,022**	**Any intracranial metastasis N = 512**
Sex			
Male	4,699 (54%)	485 (45%)	355 (69%)
Female	4,044 (46%)	589 (55%)	157 (31%)
Age at diagnosis[1]	74 (69, 80)	70 (66, 74)	73 (68, 77)
Race/Ethnicity			
Non-Hispanic White	7,572 (87%)	799 (78%)	236 (98%)
Non-Hispanic Black	307 (3.5%)	62 (6.1%)	< 16 cases
Non-Hispanic Other	315 (3.6%)	--	< 16 cases
Hispanic	549 (6.3%)	--	< 16 cases
Received Temozolomide (GBM only)			
No	4,535 (52%)	N/A	N/A
Yes	4,208 (48%)	N/A	N/A
Received Radiation			
No	3,347 (38%)	181 (18%)	193 (38%)
Yes	5,396 (62%)	841 (82%)	319 (62%)
Received Surgery			
No	2,411 (28%)	944 (92%)	251 (49%)
Yes	6,332 (72%)	78 (7.6%)	261 (51%)
Size of Surgical Excision (melanoma only)			
<3.1 cm	N/A	N/A	238 (46%)
>3.0 cm	N/A	N/A	70 (14%)
None/Unknown	N/A	N/A	204 (40%)
Beta-blocker and Checkpoint Inhibitor Use			
Checkpoint Inhibitor Only	N/A	807 (75%)	408 (80%)
Beta-blocker and Checkpoint Inhibitor	N/A	267 (25%)	104 (20%)
Beta-blocker Use			
No Beta-blocker	8,088 (93%)	807 (75%)	408 (80%)
Beta-blocker	655 (7.5%)	267 (25%)	104 (20%)
Comorbidity Score			

0	4,654 (53%)	568 (56%)	297 (58%)
1	1,854 (21%)	268 (26%)	110 (21%)
2	1,049 (12%)	95 (9.3%)	56 (11%)
3+	1,186 (14%)	91 (8.9%)	49 (9.6%)

Table 3. Cox Proportional Hazards Models and 95% Confidence Intervals (CI) Among Glioblastoma, Lung Cancer, and Melanoma Cases by Metastases in SEER-Medicare, 2008-2017

Glioblastoma				
Characteristic	**N**	**HR**	**95% CI**	**p-value**
Patient Age	8,743	1.04	1.04, 1.05	**<0.001**
Sex				
Male	4,699	—	—	Reference
Female	4,044	1.00	0.96, 1.05	0.856
Race/Ethnicity				
Non-Hispanic White	7,572	—	—	Reference
Hispanic	549	0.97	0.89, 1.06	0.453
Non-Hispanic Black	307	0.83	0.74, 0.93	**0.002**
Non-Hispanic Other	315	0.83	0.74, 0.93	<**0.001**
Had prescription records for beta-blockers				
No	8,088	—	—	Reference
Yes	655	0.64	0.59, 0.69	**<0.001**
Primary site				
Supratentorial	6,675	—	—	Reference
Infratentorial	59	0.71	0.55, 0.92	**0.010**
Other	1,256	1.12	1.05, 1.19	<**0.001**
Unspecified	753	1.37	1.27, 1.48	<**0.001**
Received Surgery of primary				
No	2,411	—	—	Reference
Yes	6,332	0.67	0.64, 0.71	**<0.001**
Received Radiation				
No	3,347	—	—	Reference
Yes	5,396	0.50	0.48, 0.52	<**0.001**

	Lung Cancer: Any intracranial metastasis			
Characteristic	**N**	**HR[1]**	**95% CI[1]**	**p-value**
Patient Age	1,074	1.01	1.00, 1.02	0.081
Sex				
Male	485	—	—	Reference
Female	589	0.74	0.65, 0.85	**<0.001**
Race/Ethnicity				
Non-Hispanic White	832	—	—	Reference
Hispanic	53	0.65	0.46, 0.91	**0.012**
Non-Hispanic Black	69	0.89	0.67, 1.18	0.421
Non-Hispanic Other	120	0.94	0.76, 1.17	0.587
Received surgery of primary				
No	995	—	—	Reference
Yes	79	0.59	0.44, 0.77	**<0.001**
Received radiation				
No	205	—	—	Reference
Yes	869	0.92	0.77, 1.08	0.310
Charlson Score				
0	611	—	—	Reference
1	272	1.04	1.00, 1.31	0.572
2	98	1.04	0.96, 1.41	0.699
3+	93	1.20	1.02, 1.51	0.167
Betablocker and Checkpoint Inhibitor Use				
Checkpoint Inhibitor Only	807	—	—	Reference
Checkpoint inhibitor and beta-blocker	267	0.80	0.68, 0.93	**<0.001**

	Melanoma: Any intracranial metastasis			
Characteristic	**N**	**HR**	**95% CI**	**p-value**
Patient Age	512	1.05	1.03, 1.06	**<0.001**
Sex				
Male	355	—	—	Reference
Female	157	0.94	0.76, 1.18	0.610
Race/Ethnicity				
Non-Hispanic White	493	—	—	Reference
Hispanic	< 16 cases	—	—	—
Non-Hispanic Black	< 16 cases	—	—	—
Non-Hispanic Other	< 16 cases	—	—	—
Surgery Size				
None/Unknown	204	—	—	Reference
<3.1 cm	238	0.50	0.40, 0.63	**<0.001**
>3.0 cm	70	0.52	0.37, 0.73	**<0.001**
Received surgery of primary				
No	251	—	—	Reference
Yes	261	0.75	0.61, 0.93	**0.008**
Received radiation				
None	193	—	—	Reference
Yes	319	1.26	1.02, 1.55	**0.033**
Charlson Score				
0	297	—	—	Reference
1	110	1.16	0.90, 1.49	0.249
2	56	1.44	1.05, 1.97	**0.023**
3+	49	1.48	1.05, 2.10	**0.026**
Beta-blocker and Checkpoint Inhibitor Use				
Checkpoint Inhibitor Only	408	—	—	Reference
Checkpoint inhibitor and beta-blocker	104	0.70	0.54, 0.91	**0.007**

-- Fewer than 16 cases or those that can be back calculated to fewer than 16 have been suppressed.
Abbreviations: SEER, Surveillance, Epidemiology, and End Results; NH, non-Hispanic; HR, hazard ratio

[1] Median (IQR)

-- Fewer than 16 cases or those that can be back calculated to fewer than 16 have been suppressed.

Abbreviations: SEER, Surveillance, Epidemiology, and End Results; NH, non-Hispanic; N/A, Not applicable; NSCLC, non-small cell lung cancer; SCLC, small cell lung cancer

Main Figures:

Intracranial tumors elicit systemic sympathetic hyperactivity that limits immunotherapeutic responses

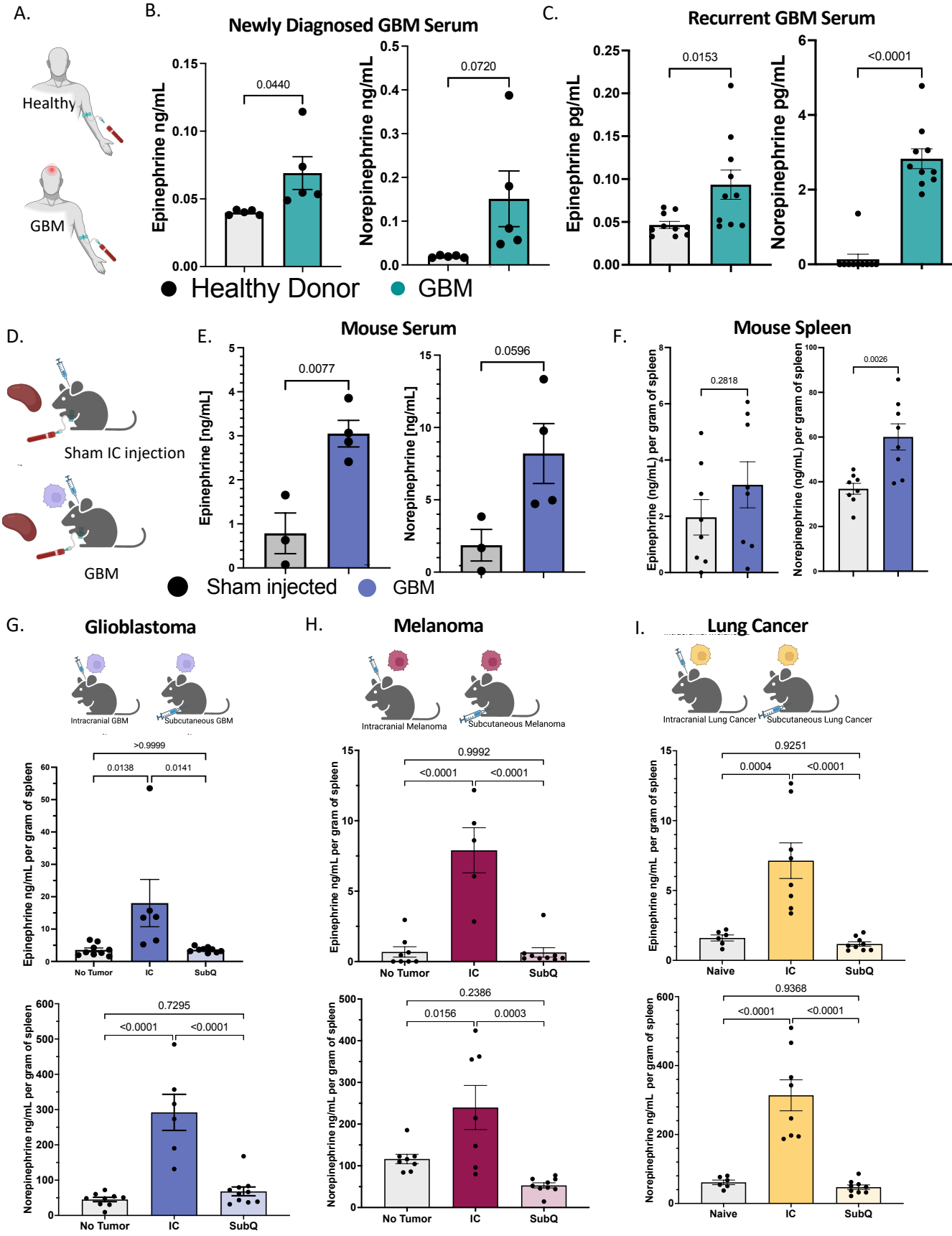

Figure 1- Patients and mice with intracranial tumors exhibit elevated systemic catecholamine levels. A. Schematic of serum collection from patients with glioblastoma or healthy controls **B.** Serum epinephrine and norepinephrine levels in patients with newly-diagnosed glioblastoma compared with healthy controls (n=5 per group). **C.** Serum epinephrine and norepinephrine levels in patients with recurrent glioblastoma compared with healthy controls (n=10 per group). **D.** Schematic of serum collected from mice with intracranial glioblastoma or a sham intracranial injection. **E.** Serum epinephrine and norepinephrine levels in mice with intracranial glioblastoma compared with a sham intracranial injection (n≥3 per group). **F.** Splenic epinephrine and norepinephrine levels in mice with intracranial glioblastoma compared with a sham intracranial injection (n=8 per group). **G.** Splenic epinephrine and norepinephrine levels in mice with no tumor, intracranial glioblastoma or subcutaneous glioblastoma (n≥6 per group). **H.** Splenic epinephrine and norepinephrine levels in mice with no tumor, intracranial melanoma or subcutaneous melanoma (n≥7 per group). **I.** Splenic epinephrine and norepinephrine levels in mice with no tumor, intracranial lung cancer and subcutaneous lung cancer (n≥6 per group). The p values in **B, C, E, F** was calculated with an unpaired T-tests and the p values in **G-I** were calculated using one-way ANOVAs and Tukey's multiple comparisons tests. Error bars denote the standard error of the mean (SEM). Data are representative of individual experiments.

A

GEO Accession	Tissue type
GSE182109	2 low grade glioma 10 newly diagnosed GBM 5 recurrent GBM
GSE154795	14 newly diagnosed GBM 12 recurrent GBM 5 PBMCs from recurrent GBM patients 2 healthy donor PBMCs
GSE160189	5 normal brain
GSE200218	5 melanoma brain metastases
GSE186344	3 breast cancer brain metastases 3 lung cancer brain metastases 3 melanoma brain metastases

Total: 69 patients (552,442 cells)

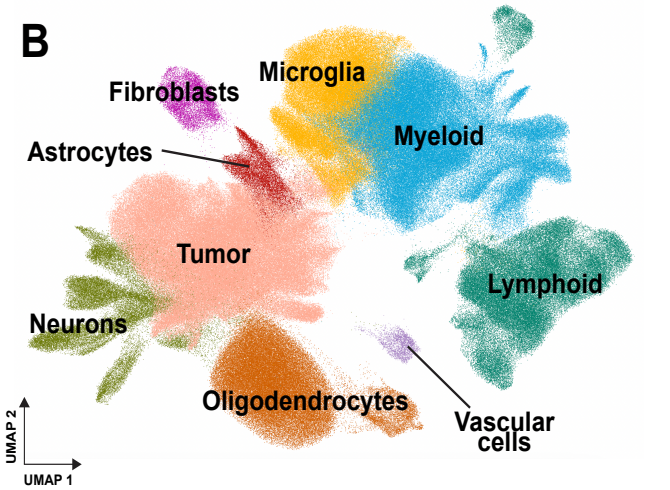

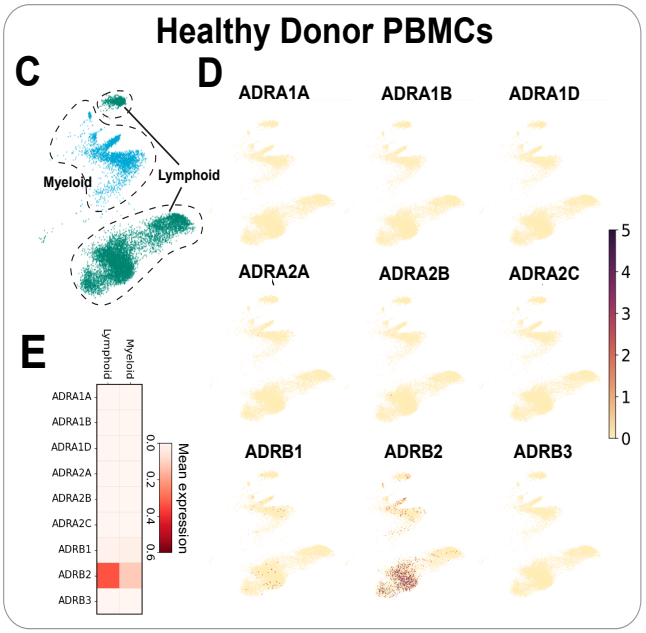

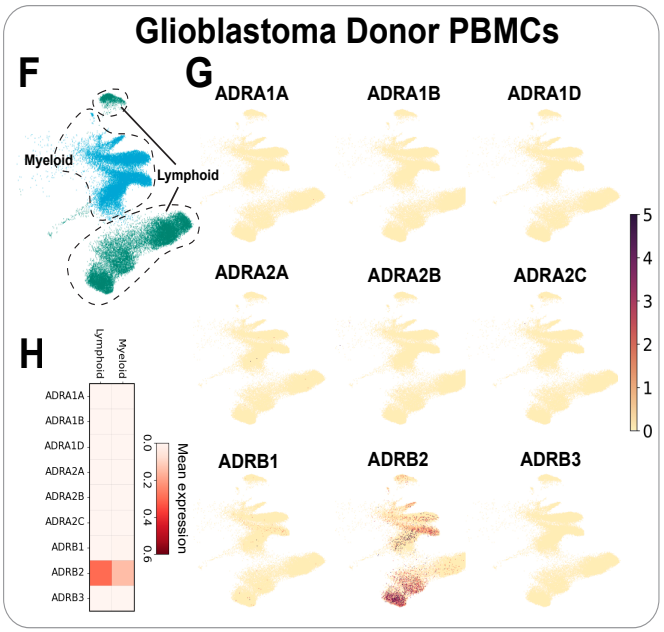

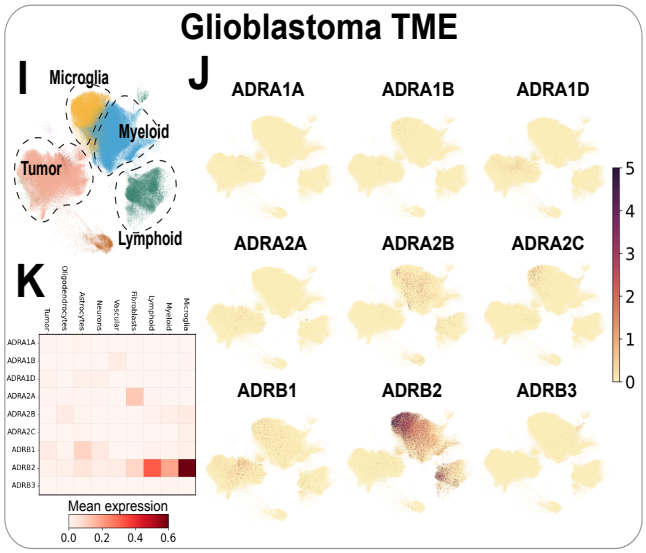

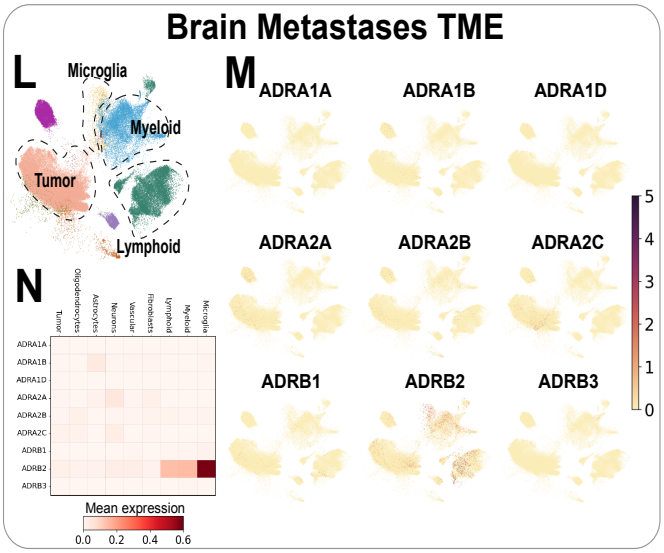

Figure 2. Beta-adrenergic, not alpha-adrenergic, receptors are expressed on systemic and TME immune cells. A. Integrated publicly available scRNAseq datasets from normal brain, glioblastoma, brain metastasis, and PBMC samples. **B.** UMAP of clusters and cell types from integrated dataset. **C.** UMAP of clusters and cell types from subsetted object only including PBMCs from healthy donors. **D.** Feature plots of adrenergic receptor expression in PBMCs from healthy donors. **E.** Heat map of adrenergic receptor expression in healthy donor PBMC cell populations. **F.** UMAP of clusters and cell types from subsetted object only including PBMCs from glioblastoma patients. **G.** Feature plots of adrenergic receptor expression in PBMCs from glioblastoma patients. **H.** Heat map of adrenergic receptor expression in glioblastoma patient PBMC cell populations. **I.** UMAP of clusters and cell types from subsetted object only including cells from glioblastoma tumor samples. **J.** Feature plots of adrenergic receptor expression in glioblastoma TME. **K.** Heat map of adrenergic receptor expression in glioblastoma TME cell populations. **L.** UMAP of clusters and cell types from subsetted object only including cells from brain metastasis samples. **M.** Feature plots of adrenergic receptor expression in brain metastasesTME. **N.** Heat map of adrenergic receptor expression in brain metastasesTME cell populations.

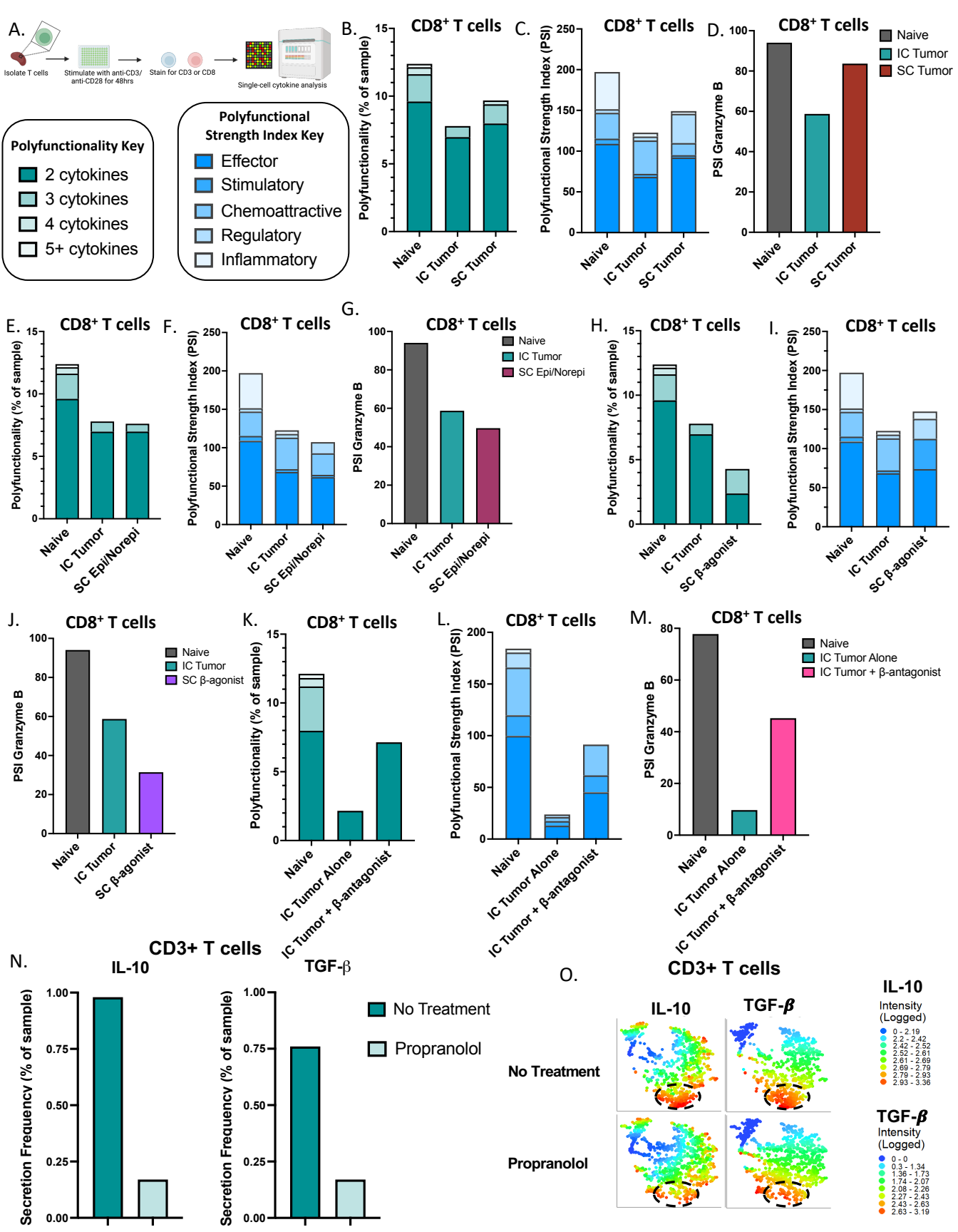

Figure 3- Both catecholamines and β-adrenergic agonism are sufficient to reduce systemic T cell function and β-adrenergic blockade restores systemic T cell function in the context of GBM A. Schematic of ELISA-based single-cell cytokine analysis **B.** Polyfunctionality and **C.** polyfunctional strength index (PSI) of various cytokine and **D.** PSI of Granzyme B from CD8+ T cells from naïve mice or mice with intracranial (IC) or subcutaneous (SC) GBM. **E.** Polyfunctionality and **F.** PSI of various cytokines, and **G.** PSI of Granzyme B from CD8+ T cells from naïve mice or mice with with IC tumors or subcutaneous pumps infusing catecholamines. **H.** Polyfunctionality and **I.** PSI of various cytokines, and **J.** PSI of Granzyme B from CD8+ T cells from naïve mice or mice with IC tumors or subcutaneous pumps infusing beta-adrenergic receptor agonist. **K.** Polyfunctionality and **L.** PSI of various cytokines and **M.** PSI of Granyzme B from CD8+ T cells from naïve mice or mice with IC tumors given no treatment or daily β-adrenergic receptor antagonist. **N.** Secretion frequency of IL-10 and TGF-β produced by naïve mice or mice with intracranial glioblastoma receiving no treatment or propranolol **O.** UMAP dimensionality reduction of IL-10 and TGF-β. N= 5 mice pooled per sample (equal number of cells from each mouse) and 30,000 cells loaded onto chip for single-cell analysis. Given the nature of these reported values as grouped outcomes from individual cells, no error bars or p values are present. Experiments for each group of single-cell cytokine analysis were performed one time.

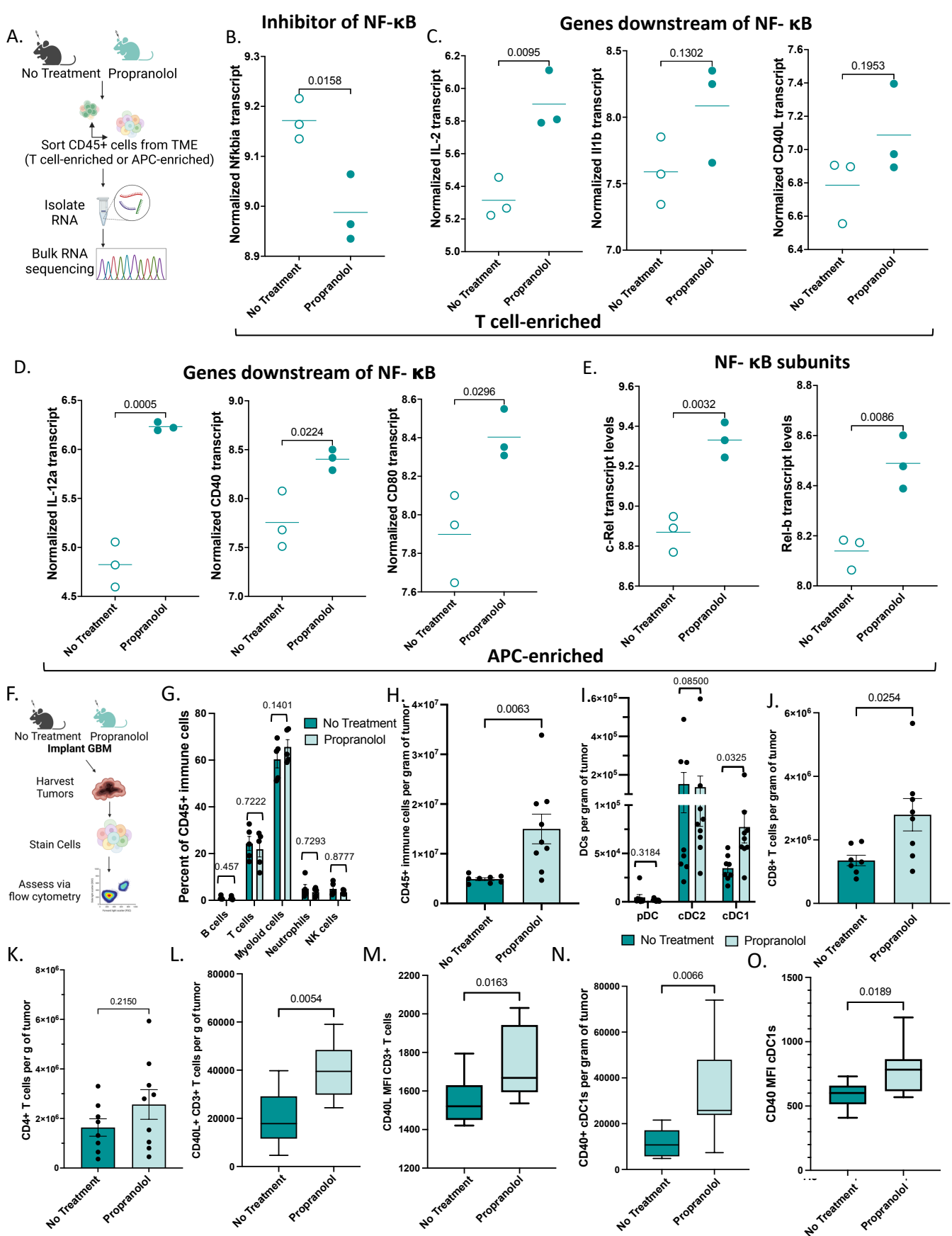

Figure 4. β-adrenergic receptor blockade favorably alters the local TME in GBM All mice were implanted with IC CT2A and tumors from 5 mice per sample were pooled (n=3 samples per group) for a total of 15 mice per group. **A.** Schematic of bulk RNA-seq analysis of immune cells enriched for T cells or antigen-presenting cells (APCs) in the TME **B.** RNA transcript levels of *Nfkbia* (IkBα), the inhibitor of NF-κB, in T cell-enriched leukocytes from the TME. **C.** Transcript levels of *IL-2, IL-1β, CD40L* genes downstream of NF-κB in T cell-enriched leukocytes from the TME. **D.** Transcript levels of downstream NF-κB genes *IL-12, CD40, CD80* in APC-enriched TILs from the TME **E.** Transcript levels of NF-kB subunits *c-Rel* and *Rel-B* in APC-enriched leukocytes from the TME**. F.** Schematic of flow cytometric analysis of immune phenotypes in the TME **G.** Characterization of tumor-infiltrating leukocytes (n=5 mice per group) **H.** Number of CD45+ immune cells per gram of tumor (n≥8 mice per group) **I.** Dendritic cell subsets per gram of tumor (n≥8 mice per group) **J.** Number of CD8+ T cells per gram of tumor (n≥7 mice per group) **K.** Number of CD4+ T cells per gram of tumor (n≥8 mice per group) **L.** Number of T cells expressing CD40L per gram of tumor (n≥7 mice per group) **M.** MFI of CD40L on T cells (n≥7 mice per group) **N.** Number of type 1 conventional dendritic cells (cDC1s) expressing CD40 per gram of tumor (n≥8 mice per group) **O.** MFI of CD40 on cDC1s (n≥8 mice per group). Unpaired T-tests were used to calculate p values. Error bars in **G-K** denote the standard error of the mean (SEM). Bars in **L-O** represent min-max. Expereiments in **G-O** were repeated independently at least 2 times; bulk RNAseq for gene expression data was performed one time.

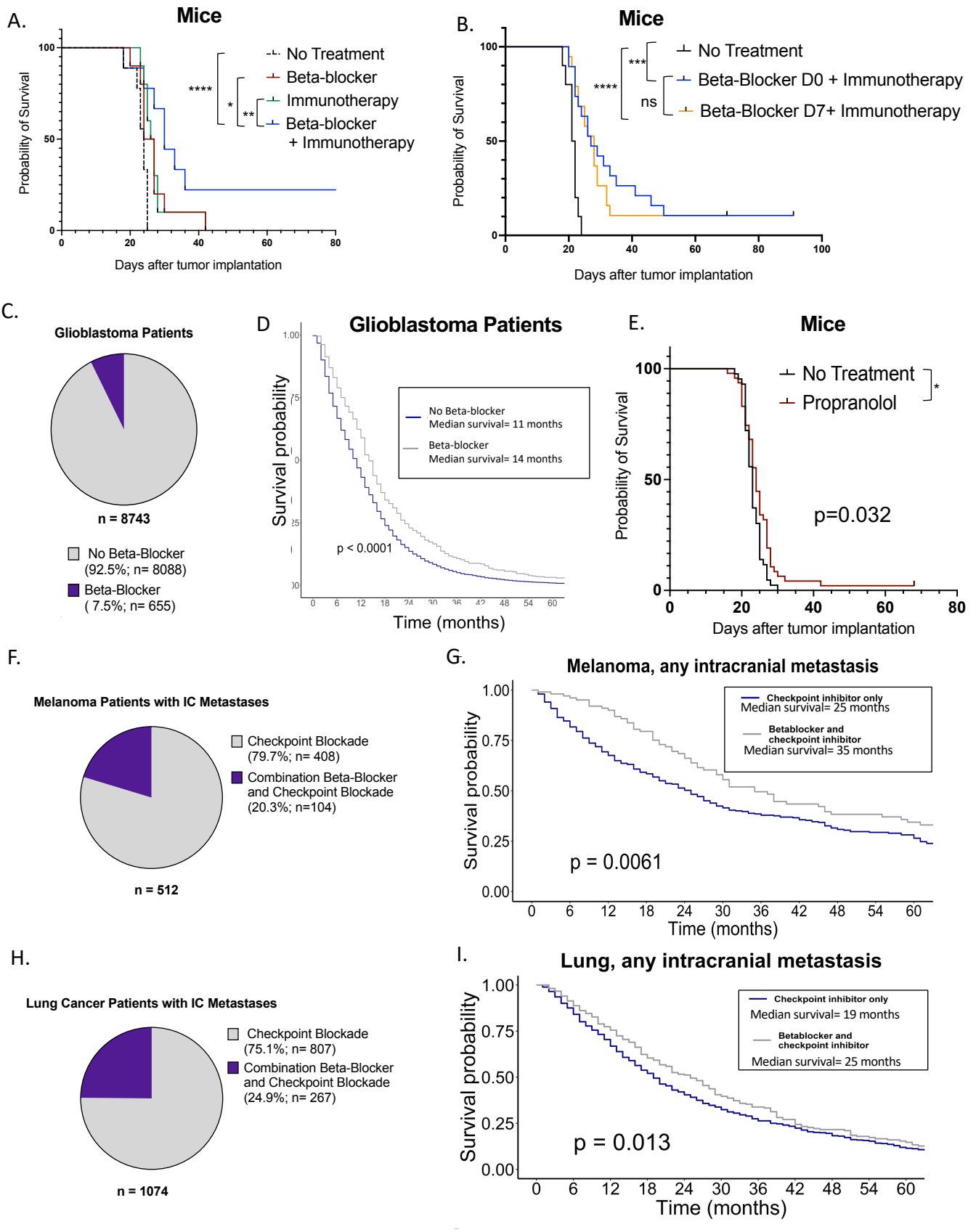

Figure 5. Repurposing β-adrenergic blockade enhances response to immunotherapy in primary and metastatic brain tumors. A. Kaplan-Meier survival curve of mice with IC CT2A receiving: no treatment , propranolol alone, immunotherapy alone, or propranolol in combination with immunotherapy (n≥10 mice per group). Immunotherapy (4-1BB) was administered 200ug/mL on days 9, 12, 15, 18. Experiment was repeated independently at least 3 times. **B.** Kaplan Meier survival curve of mice with IC CT2A receiving no treatment or a combination of 4-1BB immunotherapy and propranolol at day 0 or day 7 after tumor implantation (n≥10 mice per group per experiment and data represent pooled experiments with no exclusions) . **C.** Visual representation of total number of GBM patients retrospectively assessed for beta-blocker usage. **D.** Retrospective survival analysis of glioblastoma patients prescribed a beta-blocker or not (n= 8,723; p= <0.0001) **E.** Kaplan-Meier survival analysis of mice with IC CT2A receiving propranolol (D0) or no treatment; p=0.032 (n≥10 mice per group per experiment and data represent pooled experiments with no exclusions) **F.** Visual representation of total number of melanoma patients with brain metastases receiving checkpoint blockade and/or β-blockade **G.** Retrospective survival analysis of patients with melanoma brain metastases receiving checkpoint blockade alone or in combination with a β-blocker (n= 510, p=0.0061) **H.** Visual representation of lung cancer patients with brain metastases receiving checkpoint blockade alone or in combination with β-blockade. **I.** Retrospective survival analysis of patients with IC lung cancer metastases receiving checkpoint inhibitor alone or in combination with a **β**-blocker (n= 1,054; p=0.013). Survival was assessed via log-rank (Mantel-Cox) tests.